SURFACE FUNCTIONALIZATION OF SBA-15 PARTICLES FOR CELECOXIB DELIVERY

A THESIS SUBMITTED TO
THE GRADUATE SCHOOL OF NATURAL AND APPLIED SCIENCES
OF
MIDDLE EAST TECHNICAL UNIVERSITY

BY

GAMZE GEZER

IN PARTIAL FULFILLMENT OF THE REQUIREMENTS
FOR
THE DEGREE OF MASTER OF SCIENCE
IN
CHEMISTRY

JUNE 2013

Approval of the thesis:

SURFACE FUNCTIONALIZATION OF SBA-15 PARTICLES FOR CELECOXIB DELIVERY

submitted by **GAMZE GEZER** in partial fulfillment of the requirements for the degree of **Master of Science in Chemistry Department, Middle East Technical University** by,

Prof. Dr. Canan Özgen _____
Dean, Graduate School of **Natural and Applied Sciences**

Prof. Dr. İlker Özkan _____
Head of Department, **Chemistry**

Assoc. Prof. Dr. Ayşen Yılmaz _____
Supervisor, **Chemistry Department, METU**

Examining Committee Members:

Prof. Dr. Ceyhan Kayran _____
Chemistry Department, METU

Assoc. Prof. Dr. Ayşen Yılmaz _____
Chemistry Department, METU

Assist. Prof. Dr. Emren Nalbant Esentürk _____
Chemistry Department, METU

Assist. Prof. Dr. İrem Erel _____
Chemistry Department, METU

Assoc. Prof. Dr. Sreeparna Banerjee _____
Biological Sciences Department, METU

Date: _____

I hereby declare that all information in this document has been obtained and presented in accordance with academic rules and ethical conduct. I also declare that, as required by these rules and conduct, I have fully cited and referenced all material and results that are not original to this work.

Name, Last name: Gamze Gezer

Signature

ABSTRACT

SURFACE FUNCTIONALIZATION OF SBA-15 PARTICLES FOR CELECOXIB DELIVERY

Gezer, Gamze
M. Sc., Department of Chemistry
Supervisor: Assoc. Prof. Dr. Ayşen Yılmaz

June 2013, 72 pages

Mesoporous silica particles have been used to enhance the loading capacity of drugs into these particles, increase bioavailability and control drug release.

In this study SBA-15 particles were synthesized and functionalized to improve the loading capacity and release rate of drug. Then, drug loading and release process were investigated. Celecoxib was chosen as a model drug which is very hydrophobic. SBA-15 particles were used due to their highly ordered, well-defined mesoporous structure. These particles were modified by post-grafting method. In order to synthesize SBA-15 particles, hydrothermal synthesis method was used, Pluronic 123 triblock copolymer was used as starting material and tetraethyl orthosilicate was added as a silica source. SBA-15 samples were functionalized by post-grafting method with (3-Aminopropyl) triethoxysilane (APTES). Moreover, Boron doping of SBA-15 samples was prepared and so borosilicate samples were obtained. After functionalization process, drug loading of samples were performed with different concentration of drug in silica and to control drug release rate, release experiments results were compared.

For the characterization process of pure and drug loaded samples, X-ray Diffraction (XRD), Small-Angle X-ray Spectrometry (SAXS), N_2 adsorption-desorption, Fourier Transform Infra-red (FTIR), Elemental Analysis, Scanning Electron Microscope (SEM), Transmission Electron Microscope (TEM), Ultra-Violet Spectrometry (UV-VIS), Zeta Potential and High-Performance Liquid Chromatography (HPLC) methods were applied.

According to characterization process, amine functionalized SBA-15 samples and borosilicate samples showed the best results in loading and release experiments. For loading process amine functionalized SBA-15 particles had 61.72 % efficiency and borosilicate samples had 76.33 % efficiency. Besides, Borosilicate and amine functionalized SBA-15 samples had highest release rate of Celecoxib which were 37.57 % and 41.61 % respectively.

Functionalization process was successful to improve drug loading capacity and release rate.

Keywords: SBA-15 particles, surface functionalization, borosilicate, drug delivery systems, Celecoxib.

ÖZ

SELEKOKSİBİN SBA-15 PARÇACIKLARINA YÜKLENMESİ İÇİN YÜZEY AKTİFLEME ÇALIŞMALARI

Gezer, Gamze
Yüksek Lisans, Kimya Bölümü
Tez Yöneticisi: Doç. Dr. Ayşen Yılmaz

Haziran 2013, 72 Sayfa

Mezo gözenekli silika parçacıkları kontrollü ilaç salınımı, ilaçların biyoyararlanımlarını arttırma ve ilaçların silika parçacıklarına yüklenme kapasitelerini arttırmak amacıyla kullanılmaktadır.

Bu çalışmada ilaç yükleme kapasitesini ve ilaç salınımını arttırmak için SBA-15 parçacıkları sentezlenmesi ve yüzey aktiflenmesi yapılmıştır. Daha sonra ilaç yükleme ve salınım çalışmaları gerçekleştirilmiştir. Model ilaç olarak suda çözünmeyen Selekoksib kullanılmıştır. SBA-15 parçacıkları oldukça düzgün şekli ve düzgün gözenek boyutlarından dolayı tercih edilmiştir. SBA-15 parçacıkları sentezlemek için, başlangıç maddesi olarak Pluronic 123 kopolimer ve silika kaynağı olarak TEOS kullanılmıştır. SBA-15 parçacıklarının sentezlenmesi için hidrotermal sentez yöntemi kullanılmıştır. SBA-15 parçacıklarının yüzey aktiflenmesi APTES ile yapılmıştır ve SBA-15 parçacıklarına Bor eklenerek Borosilikat parçacıkları elde edilmiştir. Yüzey aktifleme çalışmalarından sonra değişik konsantrasyonlarda ilaç yükleme yapılarak kontrollü ilaç salınımı deneyleri gerçekleştirilmiştir.

Saf ve ilaç yüklü örneklerin karakterizasyonu X-Işınları toz kırınımı (XRD), küçük - açı X-ışınları saçılması (SAXS), N2-adsorpsiyon/desorpsiyon, fourier-transform kızılötesi (FTIR), elemental analiz, taramalı electron mikroskobu (SEM), geçirimli electron mikroskobu (TEM), ultra-viyole spektroskopi (UV-VIS), zeta potansiyel ve yüksek performans sıvı kromatografisi (HPLC) kullanılarak yapılmıştır.

Karakterizasyon sonucunda amine fonksiyonlu SBA-15 ve Borosilikat parçacıkları yükleme ve salınım deneylerinde en iyi sonuçları vermişlerdir. Yüzey fonksiyonlama ilaç yükleme kapasitesini ve salınım miktarını artırmıştır. Yükleme sonucunda amine fonksiyonlu SBA-15 parçacıkları % 61.72, Borosilikat parçacıkları % 76.33 başarıya ulaşmıştır. Ayrıca, Borosilikat ve amine fonksiyonlu SBA-15 parçacıkları % 37.57 ve % 41.61 salınım miktarı ile en yüksek salınımı göstermişlerdir.

Anahtar Sözcükler: Mezo gözenekli SBA-15 parçacıkları, yüzey aktiflenmesi, borosilikat, kontrollü ilaç salınımı, Selekoksib.

to my family…

ACKNOWLEGEMENTS

I would like to express my gratitude to my supervisor Assoc. Prof. Dr. Ayşen Yılmaz for her kind supervision, guidance, encouragement and support.

I would like to express my thanks to Prof. Dr. Sreeparna Banerjee, Prof. Dr. Leyla Yıldırım and Assist. Prof. Dr. İrem Erel for their helps and assistance during experimental process. I am also appreciative to Cansın Badan, Eda Karaarslan and Elif Arıcı for their helps and sharing a peaceful and efficient working environment in the laboratory.

I wish to express my thanks to my friends, who were always with me whenever I needed, Merve Çamsarıoğlu, Hatice Işık and Nimet & Uğur Büyükköy for their friendships and supports.

Finally my special appreciation and gratitude is devoted to my beloved family for their encouragement, love and motivation by all means.

TABLE OF CONTENT

LIST OF TABLES

TABLES

LIST OF FIGURES

FIGURES

LIST OF ABBREVATIONS

A: Absorbance
b: path length
c: concentration
ε: molar absorptivity coefficient
FTIR: Fourier-transform infra-red
GI: Gastrointestinal tract
HCl: hydrochloric acid
Å: Angstrom
HPLC: High - performance liquid chromatography
d: the distance between adjacent crystal planes
λ: wavelength of X – ray
APTES: (3 - aminopropyl) triethoxy silane
MCM: Mobil Composite Materials
BET: Brunauer - Emmett – Teller
BJH: Barrett - Joyner - Halenda trimethoxy silane
M41S: mesoporous silica family
N2: nitrogen
NH3: ammonia
DDS: drug delivery system
EtOH: ethanol
PBS: Phosphate buffer saline
TEOS: tetraethyl orthosilicate
Pluronic - 123: nonionic triblock
TEM: Transmission electron microscopy analysis
SEM: Scanning electron miscroscopy analysis
SAXS: Small - angle X- ray Scattering
UV: Ultra - violet
VIS: Visible
XRD: X-ray Diffraction
SBA: Santa Barbara Amorphous
SBA-15-C: celecoxib loaded SBA-15 sample
SBA - 15 - 1A: amine functionalized
SBA-15-A-C: celecoxib loaded amine functionalized SBA-15 sample
Borosilicate-C: celecoxib loaded Borosilicate Sample

CHAPTER 1

INTRODUCTION

Porous materials are classified according to their pore sizes; microporous, mesoporous and macroporous. Materials have pore size smaller than 2 nm are labeled as microporous, whereas materials have pore size larger than 50 nm are called as macroporous, and herein main interest is mesoporous materials which have pores in the size range of 2 and 50 nm [1].

1.1. MESOPOROUS MATERIALS

Although the most well-known porous materials are microporous zeolites, their applications are limited by their small pore size and so it was required to discover a material with a large pore size. In the early 1990s, new types of material from M41S family mesoporous materials have been synthesized [1, 2].

After the discovery of M41S family by Mobil researchers in 1992, synthesis and applications of mesoporous materials have been interested by many scientists. Ordered mesoporous materials have preferred many researchers due to their exclusive properties; highly ordered structure, tunable pore size, high surface area and good thermal stability. Moreover, these mesoporous materials have concerned for many applications such as; sensors, adsorption, catalysis and ion exchange. Even though these types of materials have used for many applications, they were not attracted for drug delivery systems until 2001. Today, intensive researches are ongoing to increase applications of ordered mesoporous materials in controlled drug delivery systems [2, 3, 4].

Mesoporous materials also get attention for drug delivery systems due to their biocompatibility. Mesoporous materials are biocompatible and nontoxic. Sarah P. Hudson and her coworkers did some experiments with animals to control the biocompatibility of mesoporous samples by using both SBA-15 and MCM-41 samples. They exhibited that mesoporous silicate particles had biocompatibility. Besides, nontoxic properties of mesoporous silicates were specified by Blumen *et al* [57].

1.2. TYPES OF MESOPOROUS MATERIALS

In order to understand different types of mesoporous materials their structures have been given below in Figure-1.

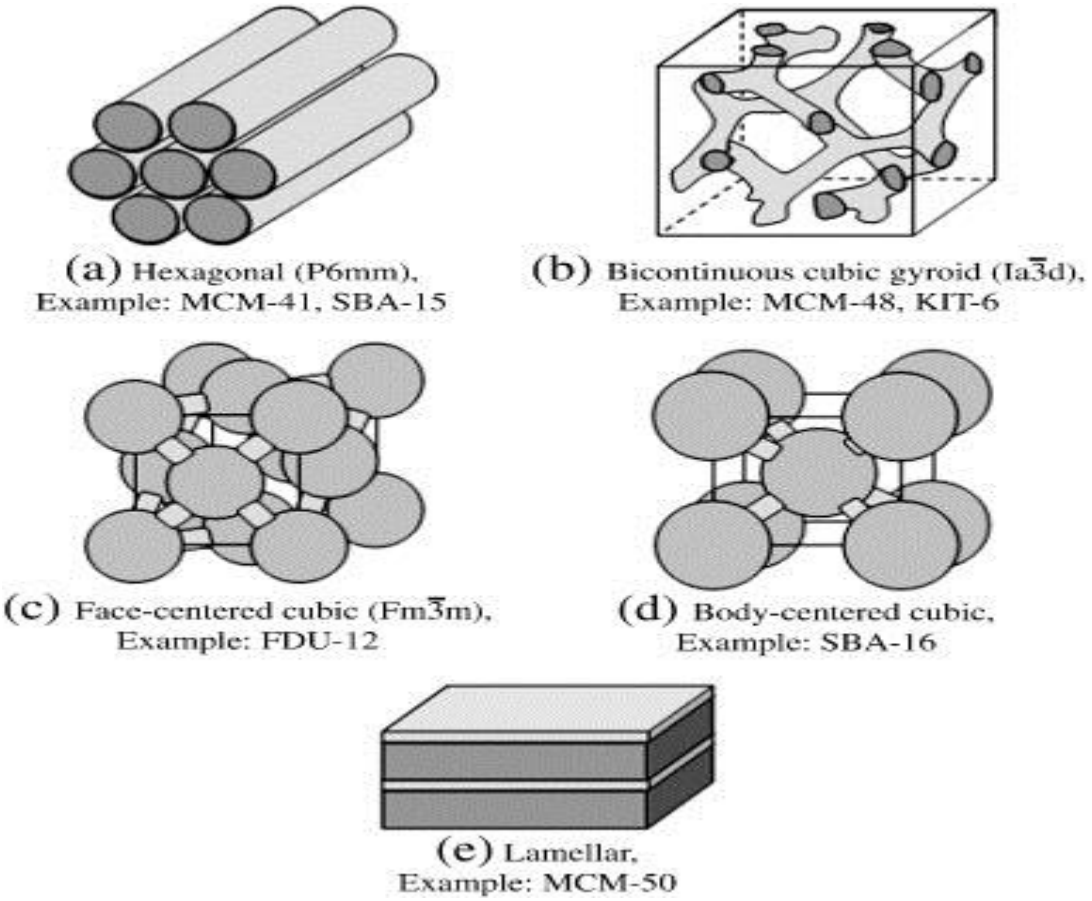

Figure-1: Structure of Mesoporous Materials [8].

1.2.1. M41S

The M41S type of silica materials are the first known mesoporous materials discovered by Kresge and collaborators. Self-assembly of surfactants structure used - the line agents form silica materials. M41S is the label of the member of several forms of MCM (Mobil Composition of Matter) materials. Different forms of M41S can be distinguished by using after the abbreviation MCM. Three of them are mostly significant: cubic MCM-48, hexagonal MCM-41 and lamellar MCM-50. M41S family materials have ordered structure and uniform pores. Quaternary ammonium salts or gemini salts are used to synthesis of these type materials. The most important considerations affecting the synthesis of M41S are the synthesis time, the carbon chain length and kind of surfactant, the hydrogel composition, the temperature and alkalinity [5].

1.2.1.1. MCM-41

MCM-41 is a mesoporous silicate which comes from M41S family with its hexagonal structure and uniforms pores [6]. It also has high surface area, large pore volume and its pores are settled in honeycomb structure. Generally, MCM-41 has a pore diameter in the range of 1.5 and 20 nm. This material has a low hydrothermal and chemical stability due to its very thin pore walls [5].

1.2.1.2. MCM-48

MCM-48 can be synthesized only surfactant to silica ratios higher than 1. MCM-48 has a cubic structure and it displays a similar surface area, pore size and volume like a MCM-41. It has also thin pore walls like a MCM-41 so its chemical and hydrothermal stability is not good. MCM-48 is a three-dimensional structured material therefore; interest of its structure has been increased [5].

1.2.2. SBA

Due to limited usage of M41S materials, highly ordered mesoporous silica materials have been discovered in 1998 by using non-ionic triblock copolymer in acidic conditions which were labeled as SBA (Santa Barbara Amorphous) types materials. These materials possess pores in the size range between 2 and 30 nm and they have different types such as SBA-11, SBA-14, SBA-15 and SBA-16. SBA-15 is the mostly used them due to its desirable features [5, 7].

1.2.2.1. SBA-15

SBA-15 has a hexagonally ordered structure with micro and meso pores. It is synthesized by using tri-block copolymer (P123) which is known as poly(ethylene glycol)-poly(propylene glycol)-poly(ethyleneglycol) and its chemical formula is $HO(CH_2CH_2O)_{20}(CH_2CH(CH_3)O)_{70}(CH_2CH_2O)_{20}H$ and it has a large surface area, large pore diameter and thick pore walls. Therefore; SBA-15 has high hydrothermal stability compared to MCM-41. The micro and mesoporous of SBA-15 particles change with experimental conditions. The tri-block copolymers have polyethylene oxide blocks which helps the formation of micropores, and polypropylene oxide which constructs mesopores [5, 7]. The schematic representation is given below in Figure-2.

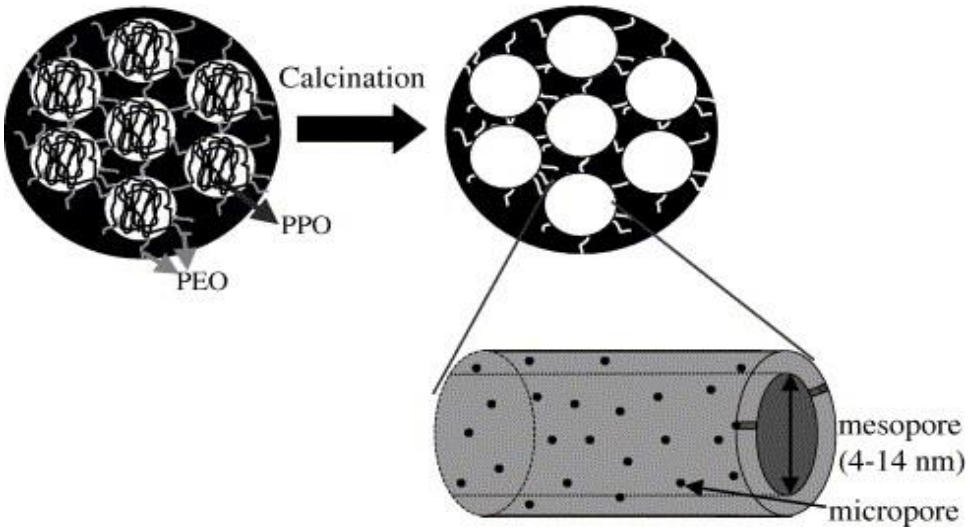

Figure-2: Schematic Representation of SBA-15 [5]

Moreover; morphology of SBA-15 particles are affected by pH, temperature, stirring rate and ionic strength [5, 7]. Due to unique properties of SBA-15 particles such as tunable pore size, ordered structure, thick pore walls, good hydrothermal stability and easy synthesis, these particles have been used in the fields of absorption, catalysis, photoluminescence, proton conductivity and controlled drug delivery systems [5, 9]. The schematic representation of tunable pore sizes of SBA-15 is given below in Figure-3.

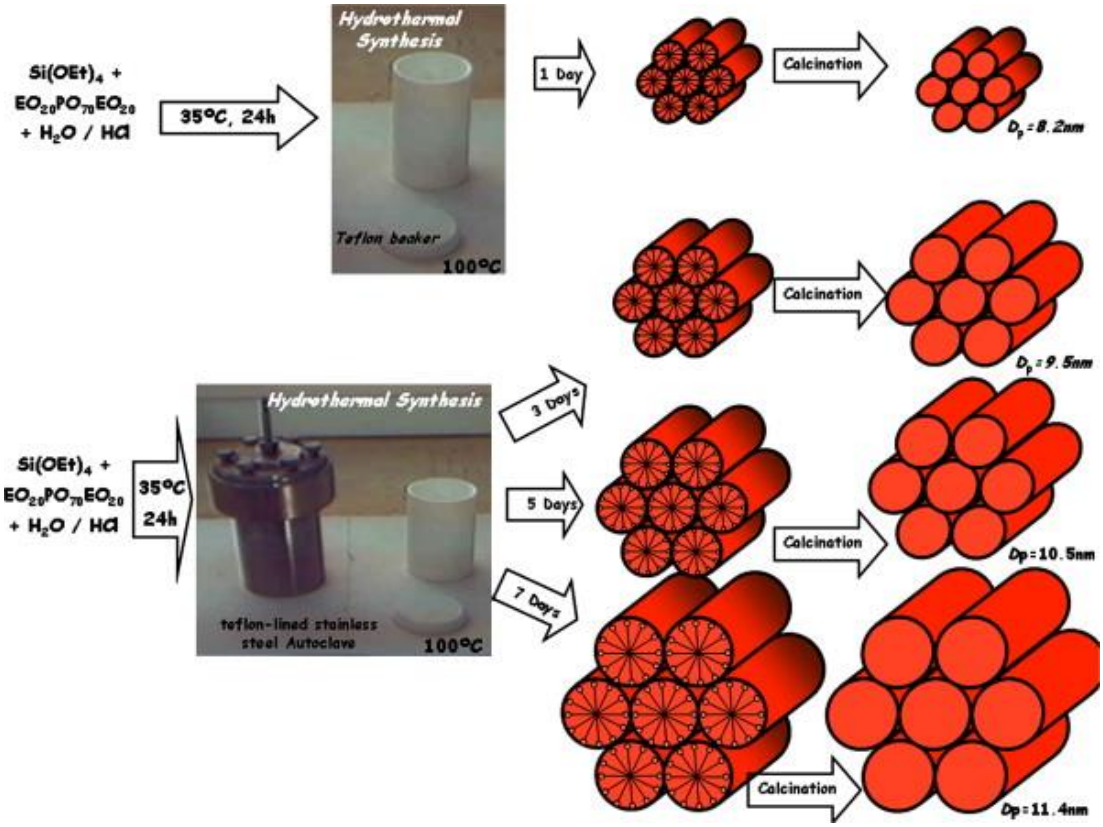

Figure-3: Scheme of Tunable Size of SBA-15 [15]

1.2.3. APPLICATIONS

After the discovery of ordered mesoporous materials, their applications has been increased several areas such as catalysis, sorption, separation, optics, sensing and drug delivery [5]. Moreover, these materials are used in repair of bone defect processes. Recently many researchers have been working on mesoporous materials for controlled drug delivery systems. Mesoporous silica nanoparticles have been used for controlled drug delivery systems by Vallet-Regi and M. Linden *et al* .They also indicated that mesoporous materials were used for drug delivery systems in cancer treatment [3, 16]. Ordered mesoporous silicates are used as a carrier in drug delivery systems due to their exclusive properties such as large surface area, pore size, good biocompatibility and easy functionalization process [10].

1.3. SYNTHESIS

The interest in synthesis of micro and meso porous materials, which are used in many applications, have been increasing due to their larger pore sizes compared to zeolites [11]. The host-guest chemistry has an important role in synthesis of mesoporous silicates. New members of mesoporous silicates can be obtained by using acid-base pairing or self-assembly of organics [12]. Moreover, by changing experimental conditions such as pH, temperature and time, different morphology of mesoporous materials can be synthesized [5].

1.4. SURFACE FUNCTIONALIZATION

Two different methods can be used for surface functionalization:

1.4.1. ONE-POT SYNTHESIS (CO-CONDENSATION)

One-Pot synthesis (direct synthesis) occurs directly when the organic groups combined with mesoporous structure. These types of reactions are dependent on co-condensation process between silica source and organosilane groups [13]. In this synthesis method, morphology of the particles can be changed by functionalization process [14].

1.4.2. POST-GRAFTING (SILYLATION)

Post-grafting synthesis method consists of reaction between organoalkoxysilanes and silanol groups. In this reaction, removal of surfactant is occurred due to prevent the reaction of organosilanes with other materials. This method is good way for surface selectivity [14].

1.4.3. ADVANTAGES AND DISADVANTAGES

Although the both synthesis methods contain the integration of organic groups within silica by organosilanes, they have some advantages and disadvantages. First of all, direct synthesis is an easy process and it has a good control capacity for loading of organosilanes. Secondly, in the one-pot synthesis functional groups concentrations are getting much more compared to post-grafting method. Therefore, post-grafting synthesis appears to be time consuming and less efficient procedure. However, post-grafting synthesis has a surface selectivity properties and this helps to interaction of mesoporous silicates during the surface functionalization [13, 14].

In drug delivery systems functionalization method is also very important. Although the direct synthesis seems to be easy way, it has some problems for drug delivery. The solubility of drug could be affected badly from direct synthesis because phase separation may not be done. Moreover; reproducibility problems could be occurred due to non-homogenous distribution of drug. Therefore; these problems can be solved by post-grafting synthesis by increasing synthesis steps and using suitable solvents [16].

Morphology of SBA-15 particles also can be changed by using functionalization process. Recently many researchers have been used pure SBA-15 for drug delivery systems, but it is not very effective. Pure SBA-15 particles contain only silanol groups and these silanol groups do not have strong hydrogen bond interaction with drugs. Therefore; to sustain efficient loading and release of drugs, surface of SBA-15 could be modified suitable functional groups [17].

1.5. CONTROLLED DRUG DELIVERY

Controlled drug delivery systems have very important role in human health. These systems are preferred instead of other techniques due to their properties such as reducing toxicity, increasing efficiency and improving suitability of patients [18]. Moreover, few amount of drug is enough to obtain good therapeutic effects in patients by using controlled release systems. Controlled drug delivery systems consist of two types. One of them is sustained delivery which proceeds over days, weeks, months or years. The other one is targeted delivery which is targeted to a tumor on a one-time. [19]. The schematic representation of controlled drug release is given below in Figure-4.

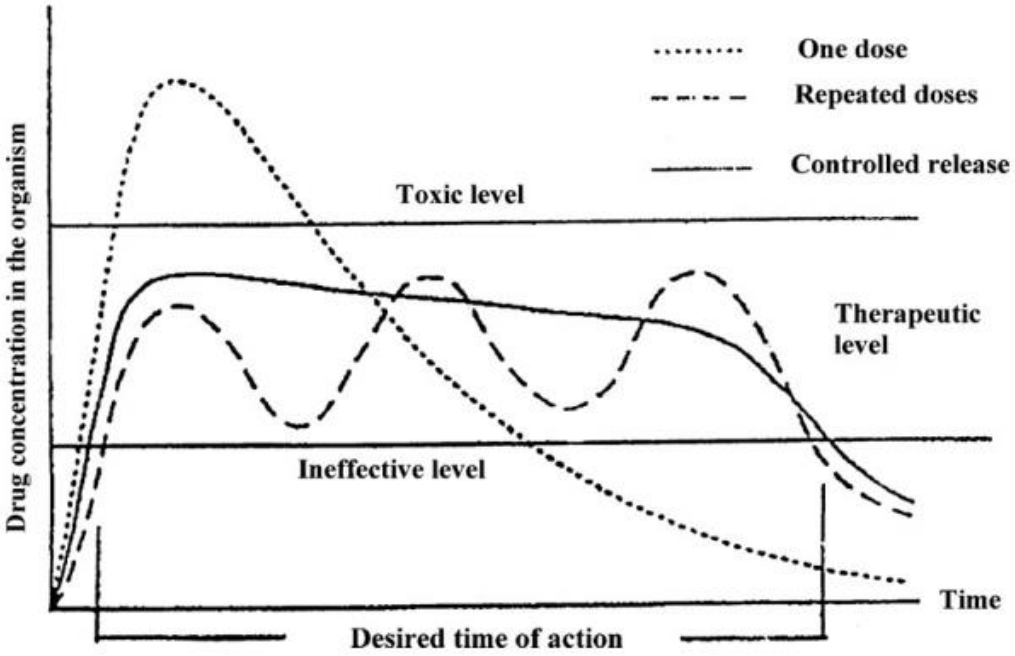

Figure-4: Graph of Controlled Drug Release [20]

1.6. DRUG DELIVERY SYSTEMS

The aim of the designing drug delivery systems (DDS) are changed the pharmacokinetics and bio-distribution of either their related drugs or to role as drug pools. Drug delivery systems have many advantages for pharmaceuticals. First of all, effect of drugs can be improved for diseases sites such as tumor targeting by using drug delivery systems. Secondly, DDS help to enhance therapeutic effects of substantial drugs. Thirdly, some new types of pharmaceuticals rising from developments in biotechnology such as proteins, plasmids or peptides does not reach target tissues or cells absence of some kinds of carrier systems [21].

Although the mostly used drug consumptions are oral administration and injection, these systems have inefficiency for some therapies. Besides, poorly soluble drugs and proteins need novel delivery systems. To overcome these problems, nanotechnology represents new materials in nano range and so they are used for many applications. Especially, silica based nano particles are used for drug delivery systems [22].

1.6.1. POLYMERIC DRUG DELIVERY SYSTEMS

The usage of polymers as drug delivery systems is well known and many polymer-based controlled drug delivery systems are designed [23]. However, polymeric systems have some problems such as poor stability, non-homogeneous dispersion and premature degradation. For that reason, inorganic drug delivery systems are investigated [24].

1.6.2. INORGANIC/ORGANIC HYBRID DRUG DELIVERY SYSTEMS

Ordered mesoporous silica materials have a significant role in controlled drug delivery systems. Well-ordered mesoporous of silicates help to homogeneous distribution of drugs during absorption and release process [22]. In the first time MCM-41 was used as a carrier of ibuprofen and its properties were controlled for controlled drug delivery systems [4]. Besides, by using functionalization process mesoporous silica surface has been changed and so drug release kinetics could be controlled according to pore-size diameter [3]. Until now MCM-41, MCM-48 and SBA-15 and their types have been used for controlled drug delivery systems [10].

1.6.3. ADVANTAGES AND DISADVANTAGES

Mesoporous silica nanoparticles have been concerned as drug delivery systems due to their stable structure, good biocompatibility, and large surface area. Moreover, surface modification of mesoporous particles alters the interaction of drugs and matrix so drug delivery rate increases [10]. Mesoporous silica particles have an important role in poorly water soluble drugs. Due to their large surface area and porosity they are appropriate for hydrophobic drugs. Besides, different from polymer-based drug delivery systems, inorganic materials can tolerate various organic solvents [25]. Mesoporous silicates also display low toxicity and good efficiency as a drug carrier system [26].

To obtain best efficiency and least toxicity loaded drugs can be protected before reaching targeted tissue. However, drug delivery systems encounter the premature drug release. Drugs loaded by electrostatic interactions or physical absorption in pores leads to altering the drugs and matrix [27].

1.7. HYDROPHOBIC DRUGS

Poorly soluble drugs show low bioavailability. They do not dissolve and absorbed completely because GI tract (Gastro Intestinal tract) reduce them. Therefore, the usage of poorly soluble drugs is restricted [28].

Although oral administration is the best way of administration, it is not suitable for poorly soluble drugs. To increase bioavailability and decrease the systemic side effect of drugs different drug delivery systems are used. These DDS consist of ordered mesoporous systems, lipid micelles or liposomes. By using these methods hydrophobic and hydrophilic surroundings are generated and so, solubility of poorly soluble drugs are improved [21, 29].

Generally, anticancer drugs have limited bioavailability because of their hydrophobic natures. Nanoparticles have an important role for drug delivery of anticancer drugs. Nanoparticles are used as drug carriers because they help to carrier of drug molecules to the targeted cells [25, 30].

1.8. CELECOXIB

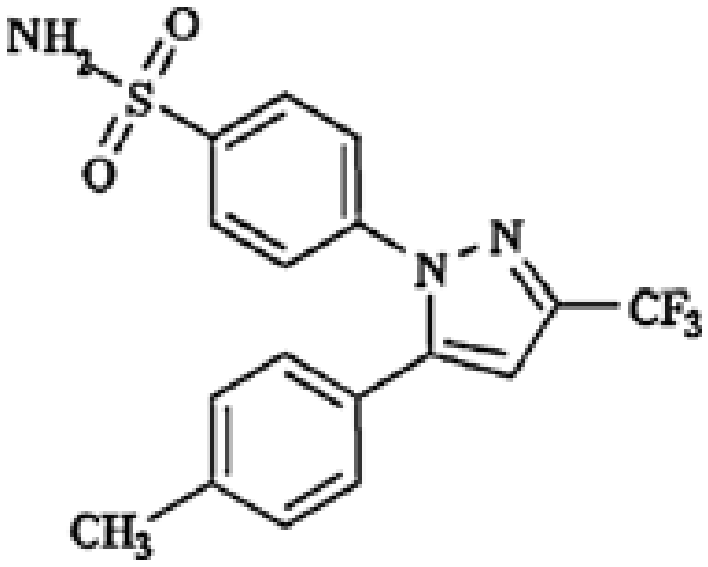

Figure-5: Structure of Celecoxib; 4-[5-(4-methylphenyl)-3-(trifluoromethyl)-1*H*-pyrazol-1-yl] benzenesulphonamide [32].

Celecoxib is an effective drug to treatment of dysmenorrhea, rheumatisim and osteoarthritis. Besides, Celecoxib is an inhibitor of COX-2 enyzme and it shows less gastrointestinal adverse effects compared to other non-steroidal anti-inflammatory drugs such as Aspirin. Recently, Celecoxib have been used as a chemo-preventive and it is a hydrophobic drug and its bioavailability is very low [32, 33]. Besides, Celecoxib have an important side effect on cardiovascular system. High dosage of Celecoxib increases the risk of cardiovascular problems [58]. However, Celecoxib has chemo-preventive property when it is used at higher dosage [33]. Therefore, in order to prevent risk of cardiovascular problem of Celecoxib drug carrier systems can be used.

In pharmaceutical industry, poor water solubility of drug is one of the most important problems because dissolution of drug is the first stage of absorption process. Therefore, pharmaceutical scientists try to improve solubility and dissolution rate of poorly soluble drugs to obtain maximum absorption [34]. However, there have been few studies about increasing the release rate of Celecoxib. In these studies, lipid-hybrid nanoparticles and fibrous ordered mesoporous carbon materials was used as a drug carriers. By using lipid-hybrid nanoparticles enzymatic digestion was controlled and absorption of compounds with poor water solubility was improved. In the other case, bioavailability of Celecoxib was enhanced and gastric irritancy was reduced by fibrous ordered mesoporous carbon [29, 34, 35].

The aim of this thesis was to overcome the poor water solubility of Celecoxib and improve its bioavailability by using SBA-15 particles. Besides, to try whether amine functionalization or boron doping would improve the loading capacity and release rate of Celecoxib.

CHAPTER 2

MATERIALS AND METHODS

2.1. MATERIALS

In this study numbers of compounds were used and they are listed in Table 1.

Table-1: List of Materials, Labels and Molecular Weights.

Chemicals	Label	Molecular Weight (g/mole)
Pluronic 123	Aldrich	5800
HCl	Sigma-Aldrich	36.46
TEOS*	Aldrich	208.33
EtOH	Sigma-Aldrich	46.07
MeOH	Merck	32.04
APTES*	Sigma-Aldrich	221.37
H_3BO_3	Merck	61.83
PBS*	---	---
H_2O	---	18.00

*TEOS: tetra ethyl orthosilicate, APTES: (3-Aminopropyl) triethoxysilane, PBS: phosphate buffer solution

2.2. INSTRUMENTATION

2.2.1. FURNACE

For all heating process occurred in Protherm furnace was used whose heating capacity up to 1300 °C with a heating control panel.

2.2.2. FOURIER TRANSFORM INFRARED SPECTROMETER (FTIR)

The FTIR spectra of samples were obtained by using Bruker IFS 66/S ATR spectrometer at Department of Chemistry. The analysis processes were done in the range of 500 to 4000 cm^{-1} and number of scan was adjusted in 128.

2.2.3. UV-VIS SPECTROMETRY

Concentration change of Celecoxib in the loading and release process were observed by using Cary-100 Bio UV-VIS Spectrometry at Department of Chemistry.

2.2.4. X-RAY DIFFRACTOMETER

The powder X-Ray diffraction data of samples were collected by using Rigaku X-Ray Diffractometer (Model, Miniflex) with CuK_{α} (30kV, 15mA, λ= 1.54051 Å). The analyses were done in 2 theta range between 1.5 and 4.0.

2.2.5. SMALL ANGLE X-RAY SCATTERING (SAXS)

Small angle X-Ray scattering measurements were accomplished in Hecus X-Ray system (Graz, Austria SWAXS) by Prof. Dr. Leyla Yıldırım at Hacettepe University. The 2 kW X-Ray source was used and for the SAXS results scattering pattern range was utilized between 0.04 and 0.550 Å.

2.2.6. TRANSMISSION ELECTRON MICROSCOPE (TEM)

The TEM analyses were done in METU Central Laboratory by using JEOL JEM 2100F STEM instrument at 80 kV. Before the analyses, samples were dissolved in ethanol in the Elma S 30 H ultrasonic bath.

2.2.7. SCANNING ELECTRON MICROSCOPE (SEM)

The SEM analyses were obtained in METU Central Laboratory by using QUANTA 400F Field Emission SEM instrument.

2.2.8. HIGH PERFORMANCE LIQUID CHROMATOGRAPHY (HPLC)

HPLC analysis was done in METU Biotechnology & Molecular Biology Central Laboratory by using Varian Prostar instrument. For the analysis, Inerstil ODS-3 C18 column (5μm x 250 mm x 4.6 mm) was used at room temperature and flow rate was adjusted 0.8 ml/min. Measurements were observed at wavelengths of 254 and 260 nm.

2.2.9. ELEMENTAL ANALYSIS

Elemental analyses were performed in METU Central Laboratory by using CHNS-932 (LECO) elemental analyzer instrument.

2.2.10. NITROGEN-SORPTION

The N_2 adsorption-desorption analysis was accomplished in METU Central Laboratory by using Quantachrome Autosorb-6 instrument. Before the analysis, all samples were heated at 200 ^{0}C for

16 hours. To calculated surface areas and pore size data, multiple point Brunauer - Emmett - Teller (BET) method and Barrett - Joyner - Halenda (BJH) method were used respectively.

2.2.11. ZETA POTENTIAL ANALYSIS

Zeta potential measurements were done by using Malvern Zetasizer Nano ZS instrument.

2.3. EXPERIMENTAL METHODS

2.3.1. SYNTHESIS OF SBA-15

4 g Pluronic 123 triblock copolymer was dissolved in 130 ml H_2O and 19.5 ml 37 % HCl solution. The prepared solution was mixed at room temperature for 75 minutes. After that, 9.5 ml TEOS, which is a source of silica, was added to this solution and temperature was increased to 40 ^{0}C. This mixture was stirred for 24 hours at 40 ^{0}C.

After 24 hours, the solution was put into the Teflon bottles for aging process. The furnace was adjusted to 80 ^{0}C and the bottles were kept at that temperature for 24 hours. Over a day, obtained solution was filtered from two different phases that were colorless solution and white precipitate. Then filtered solution was washed with water and kept to dry at ambient temperature.

When the dried sample was obtained, it was put into furnace for calcination process. In the furnace, this sample was heated at 400 ^{0}C for an hour and at 600 ^{0}C for 5 hours in the ramp rate 5 ^{0}C /min. In this process, previous synthesis method was applied [36]. The schematic representation of SBA-15 was shown in Figure-6.

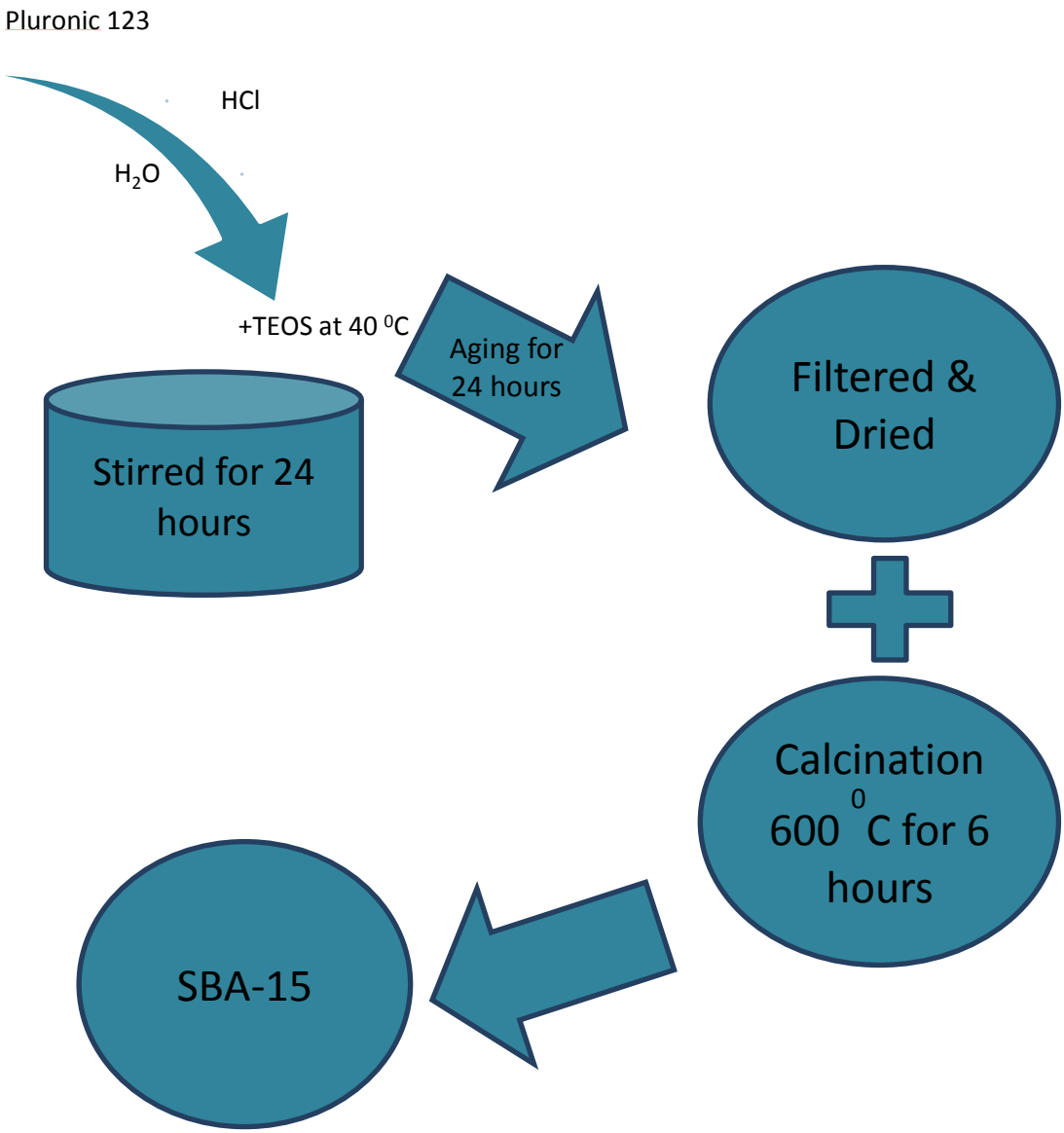

Figure-6: The Schematic Representation of Synthesis of SBA-15.

2.3.2. SYNTHESIS OF BOROSILICATE

1 g Pluronic 123 triblock copolymer was dissolved in 19 ml ethanol and 14 ml 37 % HCl solution. This solution was stirred at room temperature for 90 min. After that, 2.25 ml TEOS was added to the solution and stirred for 60 min additionally. Then 0.62 g H_3BO_3 (Si/B: 1 mole/mole) was added to the mixture and stirred about 6 hours more [37].

This prepared solution was kept at ambient temperature for 6-7 days to obtain a gel without any filtration process. The obtained gel was put into furnace at 500 ^{0}C for calcination process [37].

2.3.3. SURFACE FUNCTIONALIZATION OF SBA-15

Surface functionalization of SBA-15 was done by using APTES. 1 g of SBA-15 was taken and added 1 ml APTES. This mixture was dissolved in 50 ml ethanol. Then, prepared solution was stirred at 50 ^{0}C (±5 ^{0}C) for 6 hours [38]. To complete the functionalization process, obtained solution was filtered and dried for 2 days at room temperature. Functionalization process was summarized in Figure-7.

Figure-7: Functionalization Process of SBA-15

Surface functionalization was done because in pure SBA-15 only silanol groups exist and these silanol groups create weak hydrogen bonds with drugs. To improve the interaction capacity of silica and drug molecules the surface functionalization of SBA-15 with organic groups was needed. The SBA-15 particles were functionalized by using post-grafting method [17]. The structure of APTES functionalized sample was given below in Figure 8.

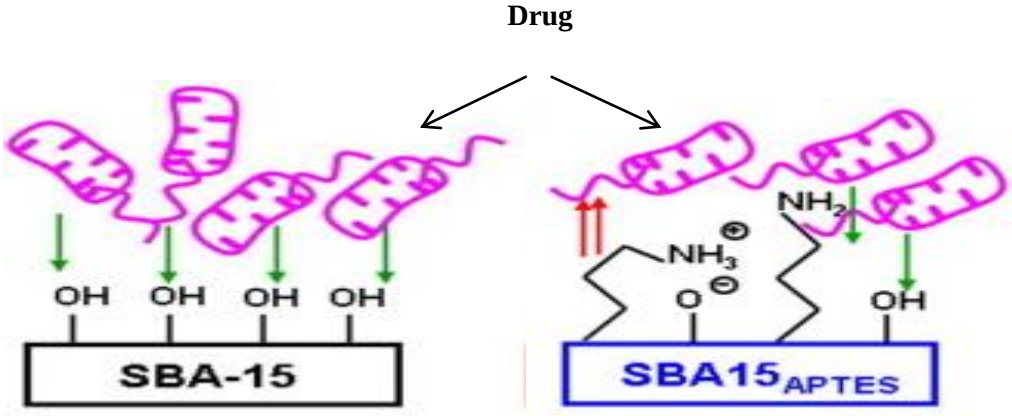

Figure-8: The Scheme of Pure and Functionalized SBA-15 [39].

2.3.4. CELECOXIB LOADING

During the Celecoxib loading process, 0.01 g SBA-15 (SBA-15+A, Borosilicate) and Celecoxib were taken and stirred in 10 ml methanol for 2 days at ambient temperature. Celecoxib loading procedure was done by using three different concentrations (Si:C: w/w) to control whether the concentration changes affects drug loading or not. These concentration differences were given in Figure-9-10-11.

Celecoxib loading was observed by using Cary-100 Bio UV-VIS Spectrometry. Loading of Celecoxib was done for 2 days and so; measurements were performed different time length: 4 hours, 8 hours, 24 hours, 32 hours and 48 hours. While the measurements wavelength interval was adjust between 200 and 500 nm and absorption peaks for Celecoxib were detected in 254 nm.

(A refers to amine functionalized sample, C refers to Celecoxib)

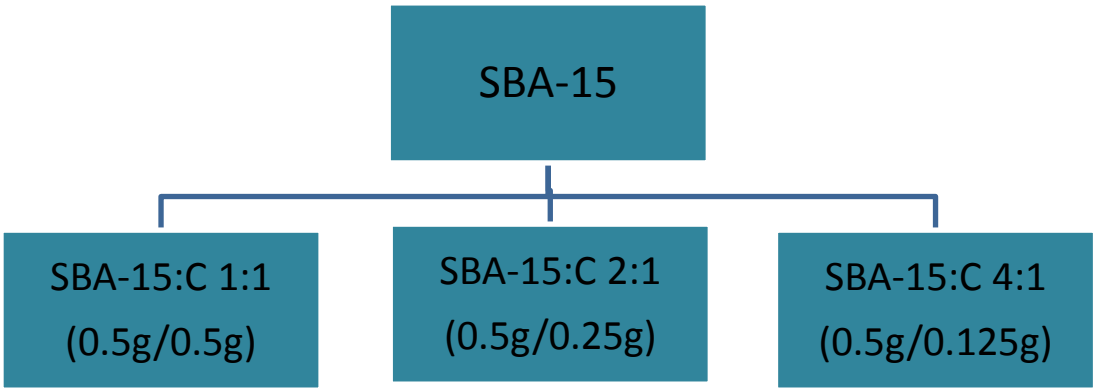

Figure-9: The Scheme of Different Concentration of Celecoxib Loaded SBA-15

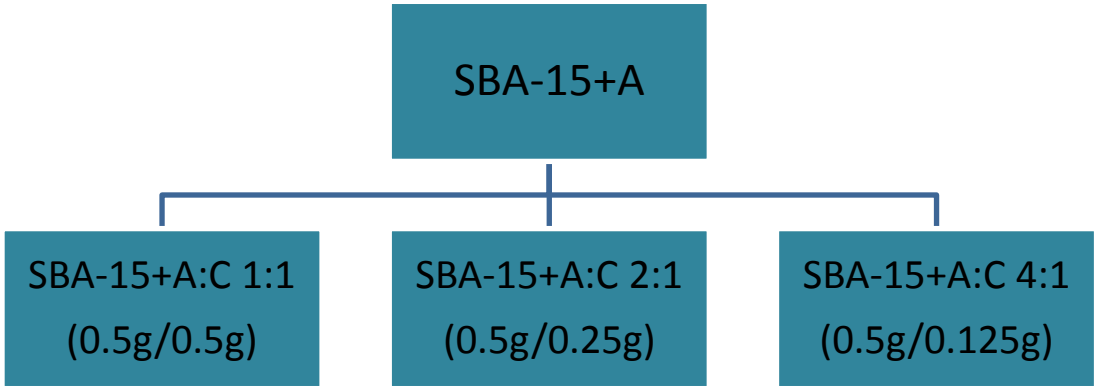

Figure-10: The Scheme of Different Concentration of Celecoxib Loaded SBA-15+APTES

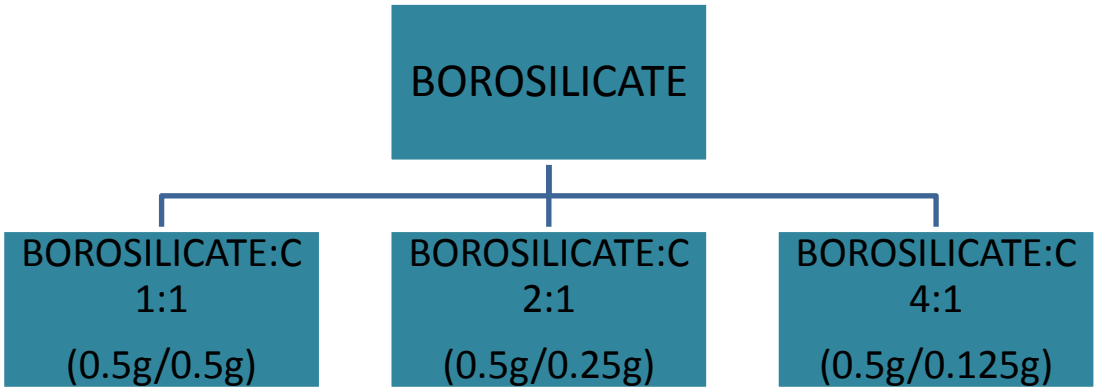

Figure-11: The Scheme of Different Concentration of Celecoxib Loaded Borosilicate

2.3.5. CELECOXIB RELEASE

Celecoxib release process was done by using two different methods.

a. UV ANALYSIS:

0.01 g Celecoxib loaded SBA-15 (SBA-15+A, Borosilicate) samples were mixed in 10 ml phosphate buffer solution and stirred within the time interval of 6 hours. Then, these solutions were centrifuged and precipitates dissolved in 10 ml of methanol. Release capacity of Celecoxib was obtained at wavelength of 254 nm by using concentration changes within the time interval of 6 hours: 30 minutes, 1 hour, 2 hours, 4 hours and 6 hours [40, 41].

b. HPLC ANALYSIS:

In order to perform HPLC analysis, 0.01 g Celecoxib loaded SBA-15 (SBA-15+A, Borosilicate) samples were mixed in phosphate buffer solution. Then, these samples were dried under vacuum and dissolved again in methanol. For the analysis 85:15 (v/v) methanol-water mobile phase was used and detection of samples were done at the wavelengths of 254 nm and 260nm [59].

CHAPTER 3

RESULTS AND DISCUSSION

SBA-15 particles were synthesized and functionalized to improve the loading capacity and release rate of drug. Then, drug loading and release process were investigated. SBA-15 samples were functionalized by post-grafting method with (3-Aminopropyl) triethoxysilane (APTES). Moreover, Boron doping of SBA-15 samples was prepared and so borosilicate samples were obtained. For the characterization process of pure and drug loaded samples, X-ray Diffraction (XRD), Small-Angle X-ray Spectrometry (SAXS), N_2 adsorption-desorption analysis, Fourier Transform Infra-red (FTIR), Elemental Analysis, Scanning Electron Microscope (SEM), Transmission Electron Microscope (TEM), Ultra-Violet Spectrometry (UV-VIS), Zeta Potential and High-Performance Liquid Chromatography (HPLC) methods were applied.

3.1. POWDER X-RAY DIFFRACTION PATTERN OF SBA-15 PARTICLES

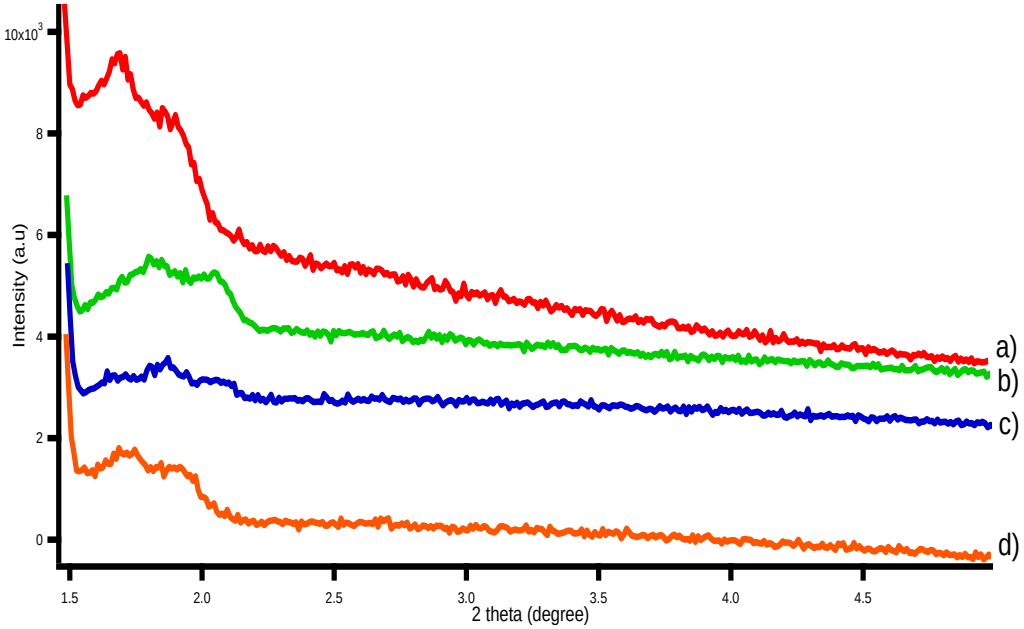

Figure-12: XRD Patterns of Celecoxib Loaded SBA-15 Particles. a) Pure SBA-15 b) SBA-15+C 1:1 c) SBA-15+C 2:1 d) SBA-15+C 4:1

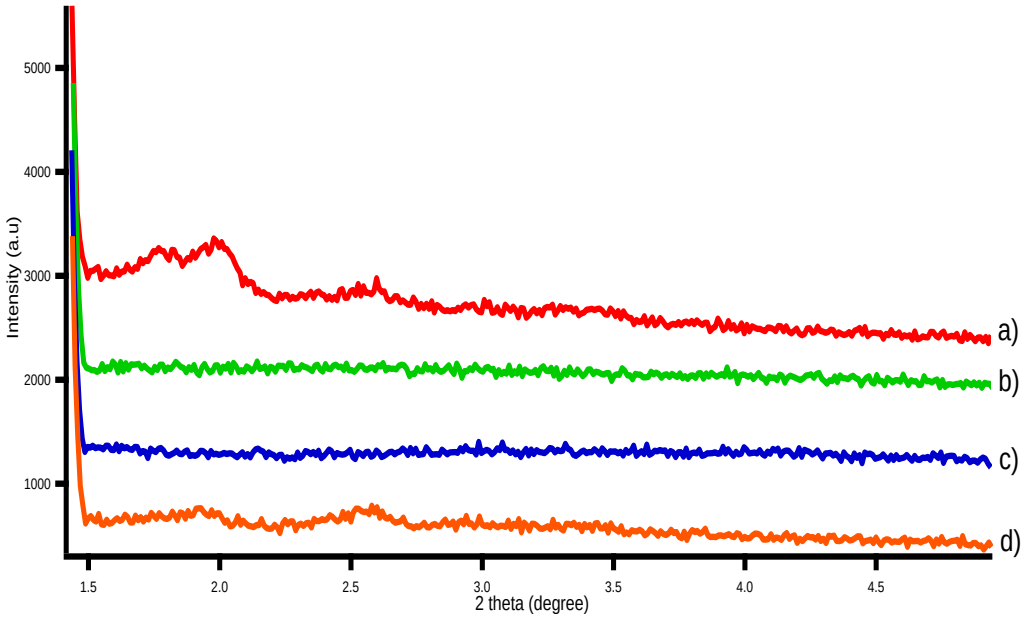

Figure-13: XRD Patterns of Celecoxib Loaded Amine Functionalized SBA-15 Particles. a) SBA-15+A b) SBA-15+A+C 1:1 c) SBA-15+A+C 2:1 d) SBA-15+A+C 4:1

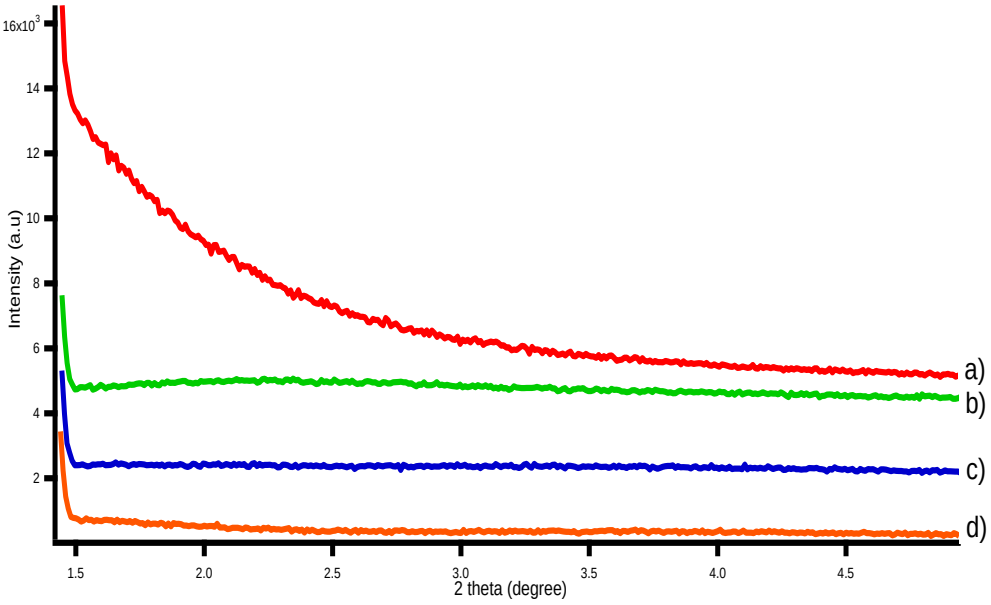

Figure-14: XRD Patterns of Celecoxib Loaded Borosilicates Particles. a) Borosilicate b) Borosilicate+C 1:1 c) Borosilicate+C 2:1 d) Borosilicate+C 4:1

Figure 12, Figure-13 and Figure 14 indicate the XRD patterns of the pure, functionalized and Celecoxib loaded SBA-15 samples. Popovici and coworkers obtained that XRD patterns of SBA-

15 types of mesoporous materials show intense peaks between 2 theta degree in 0.9 and 1.05. SBA-15 particles have also other diffraction peaks in 2 theta degree that are 1.8 and 2.0 [42]. Besides, borosilicates show intense peak at $2\theta = 0.92^{o}$ and less intense peaks at $2\theta = 1.65^{o}$ and 1.90^{o} and these values obtained by Paul *et al* [37]. According to Figure-12 SBA-15 particles had diffraction peaks at $2\theta = 1.8^{0}$ and these diffraction peaks are indexed as the planes (1 0 0), (1 1 0) and (2 0 0). These types of matrix exhibit hexagonal (P6mm) 2D structure. For the pure SBA-15 and amine functionalized samples had only one same diffraction peaks which is given in literature. For borosilicate samples which were given in Figure-14, there is no observable peak in the powder XRD pattern means there is no long range order of the pores. Besides, for amine functionalized samples SBA-15+A+C 4:1 sample was seems to have more ordered structure and this might be explained by decreasing of concentration helps to maintain ordered structure. However, not all of these peaks were observed clearly because of the instrumental limitations [37, 38, 42].

Consequently, the peaks around $2\theta = 2.0^{o}$ and 2.5^{o} having very low intensity were observed for pure and 4:1 ratio of amine functionalized SBA-15 samples. These peaks were observed after Celecoxib loading also. Therefore, these particles maintained their hexagonal structure and stability after drug loading.

3.2. SMALL ANGLE X-RAY SCATTERING (SAXS)

Small angle X-ray scattering is a useful technique to characterize hexagonally ordered SBA-15 particles. By using small angle X-ray scattering three diffraction peaks were observed in many of SBA-15 particles except borosilicate samples. The – d spacing values were calculated by using Bragg Law ($\lambda = 2d.\sin\theta$ and $q = 4\pi.\sin\theta/\lambda$). The diffraction peaks of samples were observed as (1 0 0), (1 1 0) and (2 0 0). These were characteristic of p6mm hexagonal pore structure and they have similar structures the ones reported in literature by Glatter, Khodakov and Kang *et al* [43, 44, 45].

In Table-2 d-spacing values, unit cell parameters and q- values are given.

Table-2: d- spacing, q- values and unit cell parameters of SBA-15 samples.

Sample	(hkl)	d (Å)-SAXS	q (1/ Å)	a (Å)
SBA-15	(100)	108.52	$5.79x10^{-2}$	125.41
	(110)	62.89	$9.99x10^{-2}$	
	(200)	54.17	$1.16x10^{-1}$	
SBA-15+C 1:1	(100)	107.04	$5.87x10^{-2}$	123.24
	(110)	61.60	$1.02x10^{-1}$	
	(200)	53.70	$1.17x10^{-1}$	
SBA-15+C 2:1	(100)	105.42	$5.96x10^{-2}$	121.72
	(110)	61.00	$1.03x10^{-1}$	
	(200)	52.80	$1.19x10^{-1}$	
SBA-15+C 4:1	(100)	108.52	$5.79x10^{-2}$	125.41
	(110)	62.89	$9.99x10^{-1}$	
	(200)	54.17	$1.16x10^{-1}$	
SBA-15+A	(100)	102.33	$6.14x10^{-2}$	118.25
	(110)	59.28	$1.06x10^{-1}$	
	(200)	51.08	$1.23x10^{-1}$	
SBA-15+A+C 1:1	(100)	111.9	$5.61x10^{-2}$	129.33
	(110)	----	----	
	(200)	----	----	
SBA-15+A+C 2:1	(100)	107.04	$5.87x10^{-2}$	123.54
	(110)	61.6	$1.02x10^{-1}$	
	(200)	53.70	$1.17x10^{-1}$	

Table-2: d- spacing, q- values and unit cell parameters of SBA-15 samples (cont'd).

Sample	(hkl)	d (Å)-SAXS	q (1/ Å)	a (Å)
SBA-15+A+C 4:1	(100)	102.33	$6.14x10^{-2}$	118.25
	(110)	----	----	
	(200)	----	----	
BOROSILICATE	(100)	110.23	$5.70x10^{-2}$	127.34
	(110)	----	----	
	(200)	----	----	
BOROSILICATE+C 1:1	(100)	107.04	$5.87x10^{-2}$	123.54
	(110)	----	----	
	(200)	----	----	
BOROSILICATE+C 2:1	(100)	103.85	$6.05x10^{-2}$	119.96
	(110)	----	----	
	(200)	----	----	
BOROSILICATE+C 4:1	(100)	108.52	$5.79x10^{-2}$	125.41
	(110)	----	----	
	(200)	----	----	

The d-spacing values were calculated by using diffraction peaks of SAXS patterns. They are nearly the same after functionalization process. The d-spacing value of pure SBA-15 was obtained as 10.9 nm and it is the quite similar with reported value which is 10.7 nm. Besides, 'a' parameter of pure SBA-15 particle was 12.5 nm and it was also similar with other results. After functionalization of SBA-15 samples with amine groups 'a' parameter was decreased as 11.8 nm and in the article it is given as 12.2 nm. Moreover, d- spacing value of amine functionalized sample was obtained as 10.23 nm. In borosilicate case, 'a' parameter was found as 12.73 nm and d-spacing value was 11.02 nm. In the literature d-spacing value of borosilicate was found 9.46 nm by Paul *et al* [37, 46]. Thus, the results are like as estimated. However, only 'a' parameter of SBA-15+A+C 1:1 sample was increased. It might be caused by drug would not attach to inside of the pores and due to the attachment of drug to outside of pore the wall becomes thicker to form higher unit cell dimension than pure and amine functionalized form of silica.

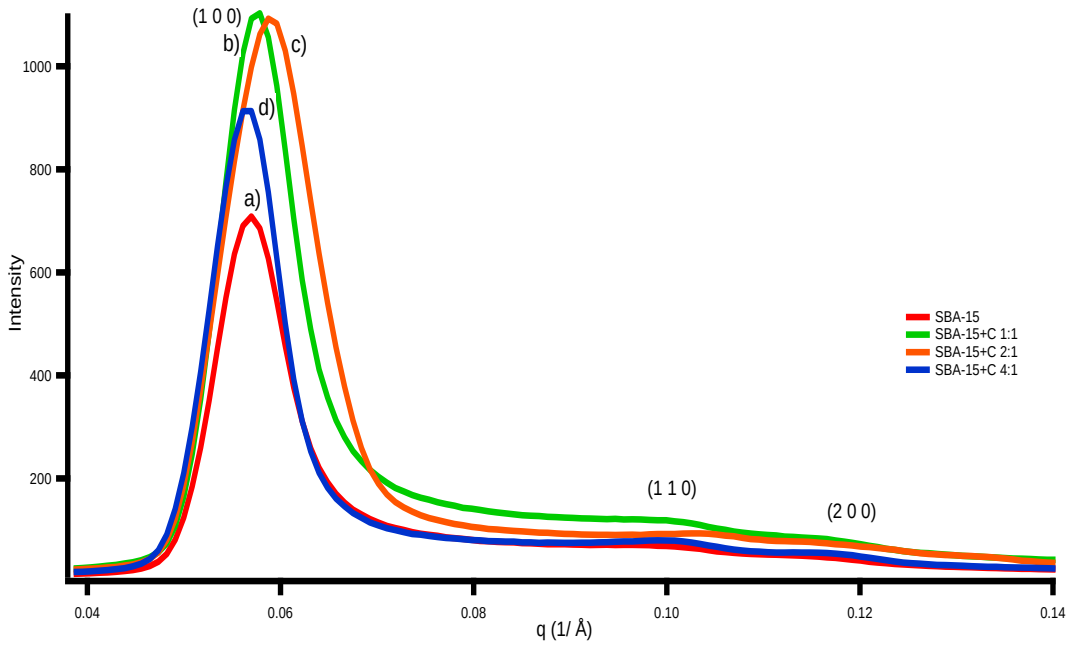

Figure-15: SAXS Patterns of SBA-15 Samples. a) SBA-15, b) SBA-15+C 1:1, c) SBA-15+C 2:1, d) SBA-15+C 4:1

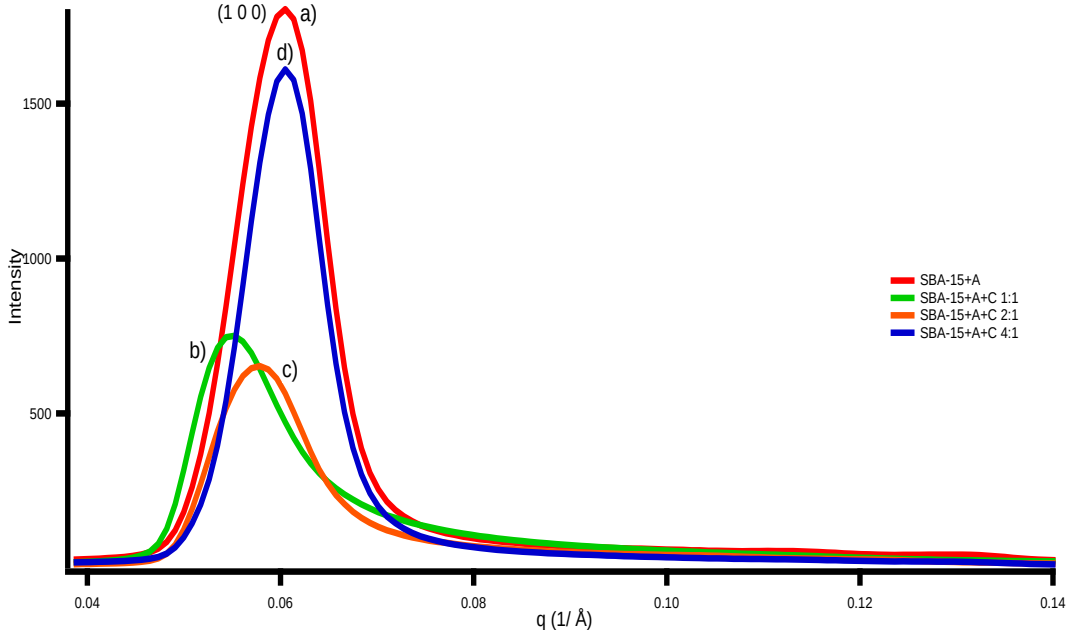

Figure-16: SAXS Patterns of Amine Functionalized SBA-15 Samples. a) SBA-15+A, b) SBA-15+A+C 1:1, c) SBA-15+A+C 2:1, d) SBA-15+A+C 4:1

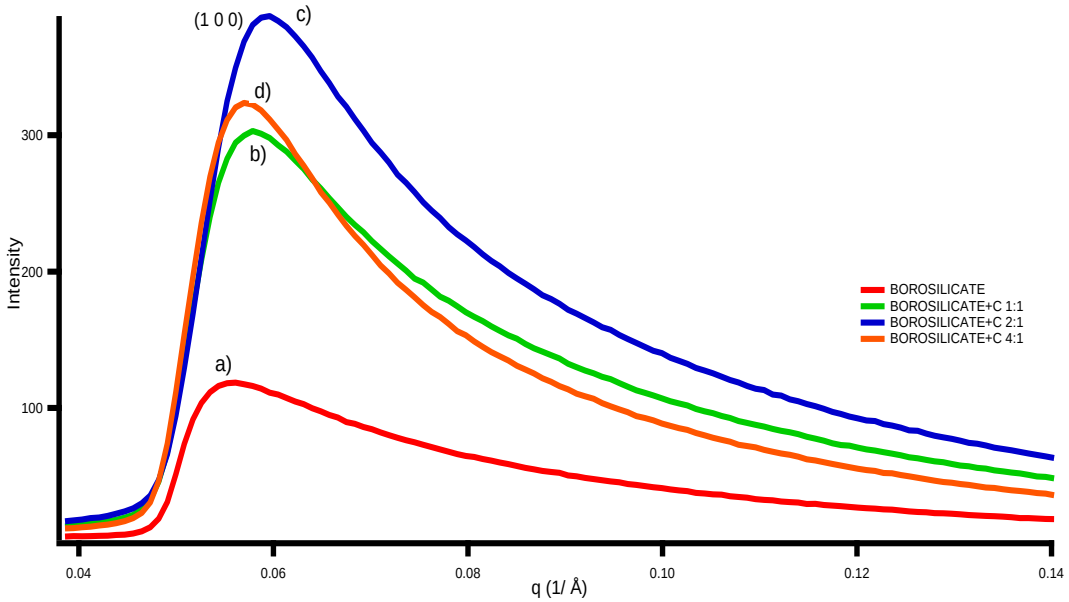

Figure-17: SAXS Patterns of Borosilicates. a) Borosilicate, b) Borosilicate+C 1:1, c) Borosilicate+C 2:1, d) Borosilicate+C 4:1

Figure-15, Figure-16 and Figure-17 indicate the SAXS graphs of SBA-15 samples, amine functionalized SBA-15 samples and borosilicate particles respectively. According to results, intensity of SBA-15 and borosilicate particles increased with loading of Celecoxib but amine functionalized SBA-15 particles showed as an opposite trend. Pure SBA-15 samples showed lower intensity in (1 1 0) and (2 0 0) which were given in Figure-15. However, these small diffraction peaks were not observed in amine functionalized SBA-15 samples and this indicate that after functionalization process ordered structure were not maintained completely. Moreover, borosilicate samples had broader peaks than SBA-15 samples. Although the SBA-15 samples had more ordered structure, amine functionalized and borosilicate samples had quite hexagonal ordered structure [38].

3.3. FTIR ANALYSIS

3.3.1. PURE, AMINE FUNCTIONALIZED SBA-15 AND BOROSILICATE SAMPLES

FTIR spectra of pure, amine functionalized SBA-15 and borosilicate samples are given in Figure-18. For SBA-15 samples there was a small band in 3000-3500 cm^{-1} which refers as silanol groups. The asymmetric NH_2 stretching band occurs in 1602 cm^{-1} but it was very small peaks. Amine functionalized SBA-15 sample had more intense peak at around 1600 cm^{-1} than pure SBA-15 sample. Besides, in 2900 cm^{-1} there was a small peak which refers to C-H stretching of

CH_2 or CH_3 and it was detected due to remaining ethoxy groups. Same results were obtained by Wong *et al* [17]. For borosilicate sample, there was a strong peak at 3420-3474 cm^{-1} which was due to O-H stretching of silanol groups and this O-H band was the most intense peak compared with pure and amine functionalized SBA-15 samples. Moreover, there was a quite strong peak at 1082 cm^{-1} due to Si-O bands. B-O stretching was also observed at near 1400-1500 cm^{-1}. In the literature, there is also some peaks at 3000-3700 cm^{-1} which refers to silanol groups and there is a small peak around 1600 cm^{-1} for NH_2 stretching in SBA-15 and amine functionalized SBA-15 sample. Besides, silanol groups showed a band around 3400 cm^{-1} and B-O stretching band at 1400-1500 cm^{-1} for borosilicate samples and they were also found by Paul *et al* [17, 37].

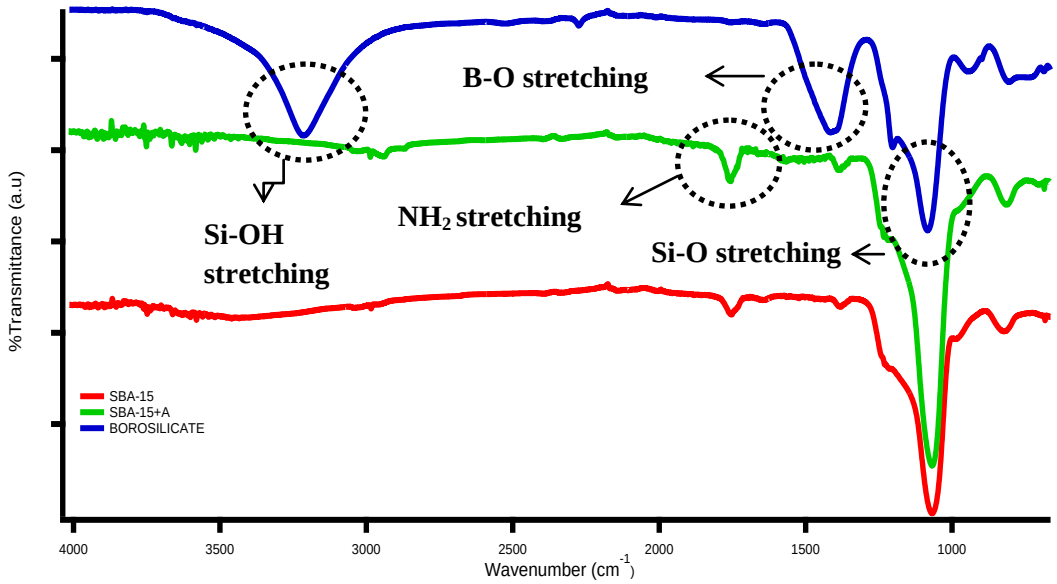

Figure-18: FTIR Spectra of SBA-15 Samples. a) SBA-15, b) SBA-15+A, c) Borosilicate

3.3.2. CELECOXIB LOADED SBA-15 SAMPLES

FTIR spectra of Celecoxib loaded pure SBA-15, amine functionalized and borosilicate samples are given in Figure-19, Figure-20 and Figure-21 respectively. Generally, Celecoxib loaded samples showed quite similar peaks with pure SBA-15 sample. There was a difference at 3000-3500 cm^{-1} and this might be linkage of drugs and SBA-15 and borosilicate samples. The intensity of Si-OH stretching was decreased for borosilicate a sample which was given in Figure-21. This showed that borosilicate sample and drug had an interaction by using Si-OH bonds. In the literature, Rayikovitch and coworkers indicated that Celecoxib gives a characteristic peak at about 3341 cm^{-1} due to N-H stretching of drug [47]. In the graphs, small peaks were observed about 3300-3400 cm^{-1} compared with pure samples. As a result, there was a difference between pure and Celecoxib loaded amine functionalized SBA-15 samples around 1600 cm^{-1}. This might

be explained by Celecoxib had a bond with NH_2 group because, after drug loading intensity of this peak about 1600 cm^{-1} was decreased which was given in Figure-20. Besides, Celecoxib loaded borosilicate samples indicated reducing in intensity of O-H peaks and this shows that Celecoxib was bonded with OH groups of borosilicate samples. However, there were not any differences in pure SBA-15 samples and so, functionalized samples showed more interaction with drug.

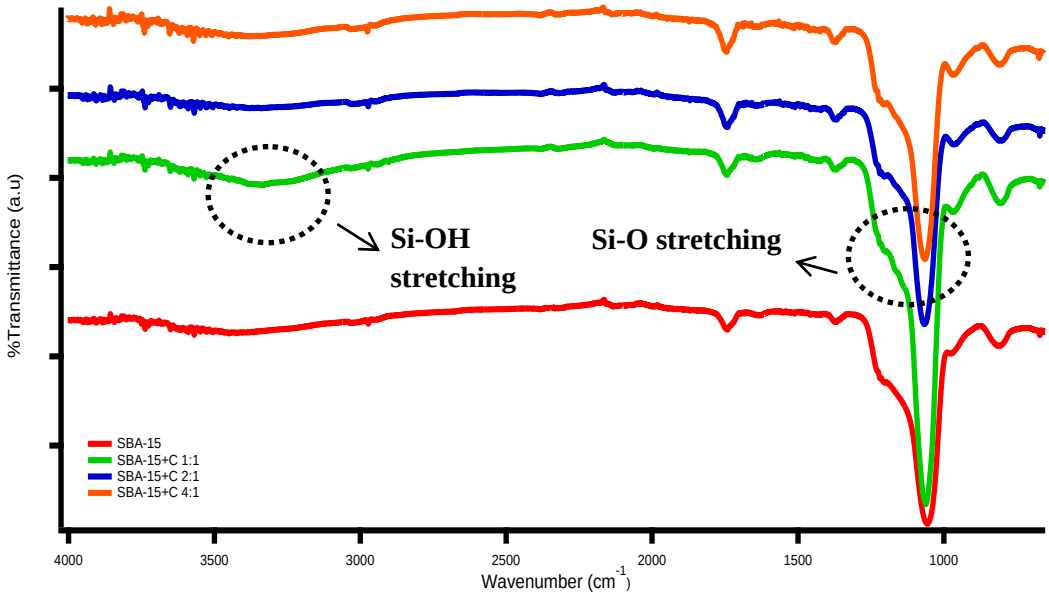

Figure-19: FTIR Spectra of Pure and Celecoxib Loaded SBA-15 Samples. a) SBA-15, b) SBA-15+C 1:1, c) SBA-15+C 2:1, d) SBA-15+C 4:1

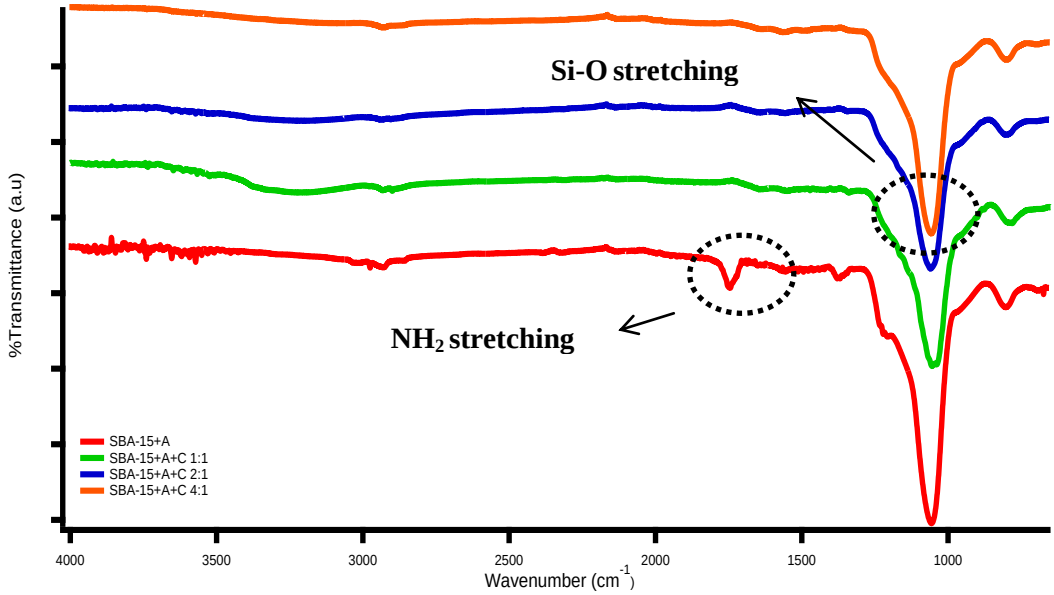

Figure-20: FTIR Spectra of Amine Functionalized and Celecoxib Loaded SBA-15 Samples. a) SBA-15+A, b) SBA-15+A+C 1:1, c) SBA-15+A+C 2:1, d) SBA-15+A+C 4:1

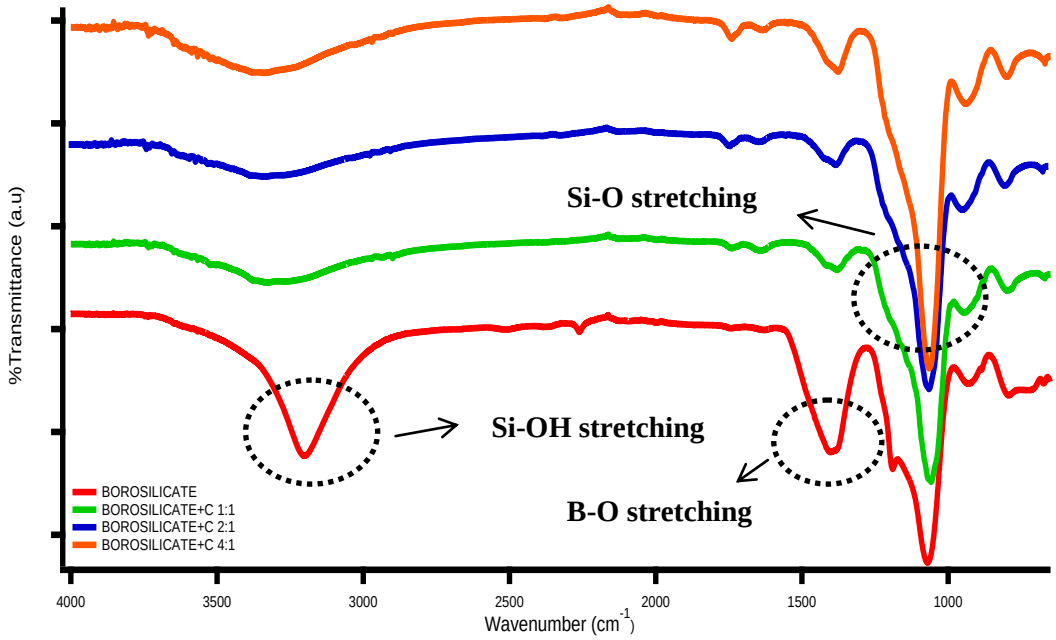

Figure-21: FTIR Spectra of Celecoxib Loaded Borosilicate Samples. a) Borosilicate, b) Borosilicate+C 1:1, c) Borosilicate+C 2:1, d) Borosilicate+C 4:1

3.4. ELEMENTAL ANALYSIS

Elemental analysis results are given in Table-3. The percent efficiency of loaded Celecoxib was calculated by using carbon percentage. According to the results, amine functionalized SBA-15 (SBA-15+A+C 2:1) had the best result with 54.91% of Celecoxib. Functionalization process seems to be good way for drug loading because amine functionalized SBA-15 and borosilicate samples indicate higher loading capacity than pure SBA-15. Besides, the amount of Celecoxib can be calculated by using UV-VIS spectroscopy. In the elemental analysis, results were obtained from the solid samples. However, loading process of Celecoxib was performed in methanol solution. Therefore, filtration process might cause the Celecoxib lost.

Table-3: Elemental Composition of Celecoxib Loaded SBA-15 and Borosilicate Samples (%C and %H).

Sample	% C	% H	% Efficiency
SBA-15+C 1:1	7.9	2.33	29.59
SBA-15+C 2:1	5.3	2.42	29.73
SBA-15+C 4:1	3.87	2.41	28.95
SBA-15+AC 1:1	11.61	3.52	43.48
SBA-15+AC 2:1	9.79	3.20	54.91
SBA-15+AC 4:1	6.12	2.77	45.77
Borosilicate+C1:1	9.54	2.56	35.73
Borosilicate+C2:1	5.44	2.03	30.51
Borosilicate+C4:1	3.63	1.80	27.15

3.5. N_2 ADSORPTION-DESORPTION ANALYSIS

3.5.1. BET ISOTHERMS

According to the pore size distribution, samples show different types of geometries of pores such as slit-like, cylindrical or ink-bottle. Mesoporous materials are known with their cylindrical pores which are described as H1 type hysteresis loop. Pure SBA-15 and amine functionalized SBA-15 samples display type IV isotherms with H1 hysteresis loop due to their highly ordered mesoporous structures [54, 55, 56].

The N_2 adsorption-desorption analysis is done to define pore size distribution at constant temperature and variety of pressures. N_2 adsorption-desorption analysis is used to obtain information about pore structure properties of mesoporous materials such as SBA-15 samples. SBA-15 particles show a H1 type hysteresis loop and it is the typical properties of mesoporous materials. Desorption and absorption of flexible mesoporous is related to this type hysteresis loop [47, 48].

The BET isotherms of pure, functionalized and Celecoxib loaded SBA-15 and borosilicate samples are given in Figure-22, Figure-23 and Figure-24. According to graphs hysteresis loops were observed where P/P_0 is between 0.4-0.8 and this also is same in literature [49]. Besides, all of the samples had a quite similar hysteresis loop shape after drug loading and so the results show that pore shapes were not changed intensely and drug release was steady [29].

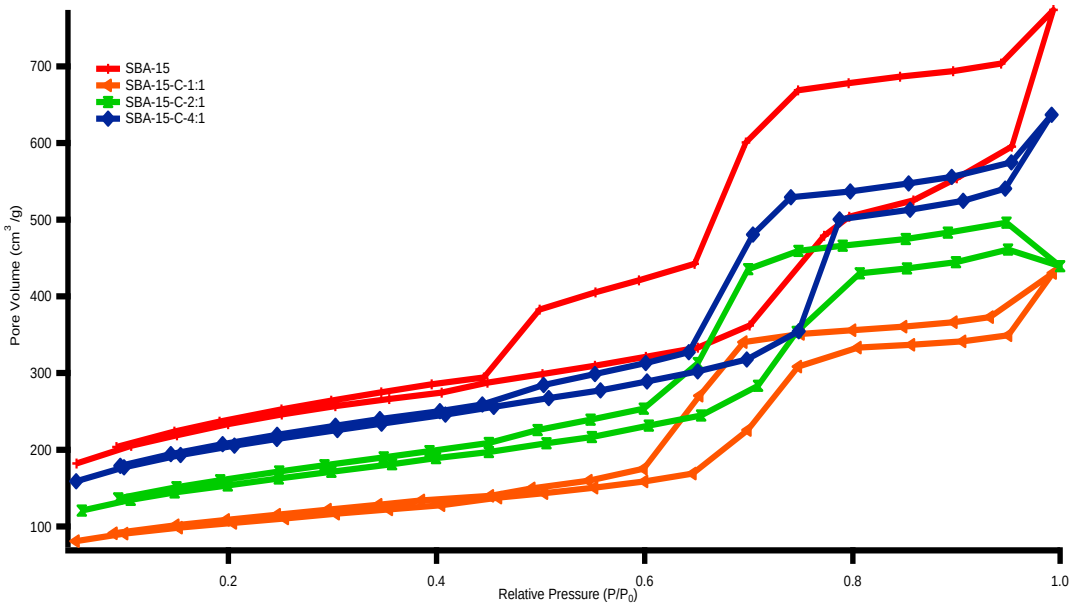

Figure-22: BET Isotherms of Pure and Celecoxib Loaded SBA-15 Particles.

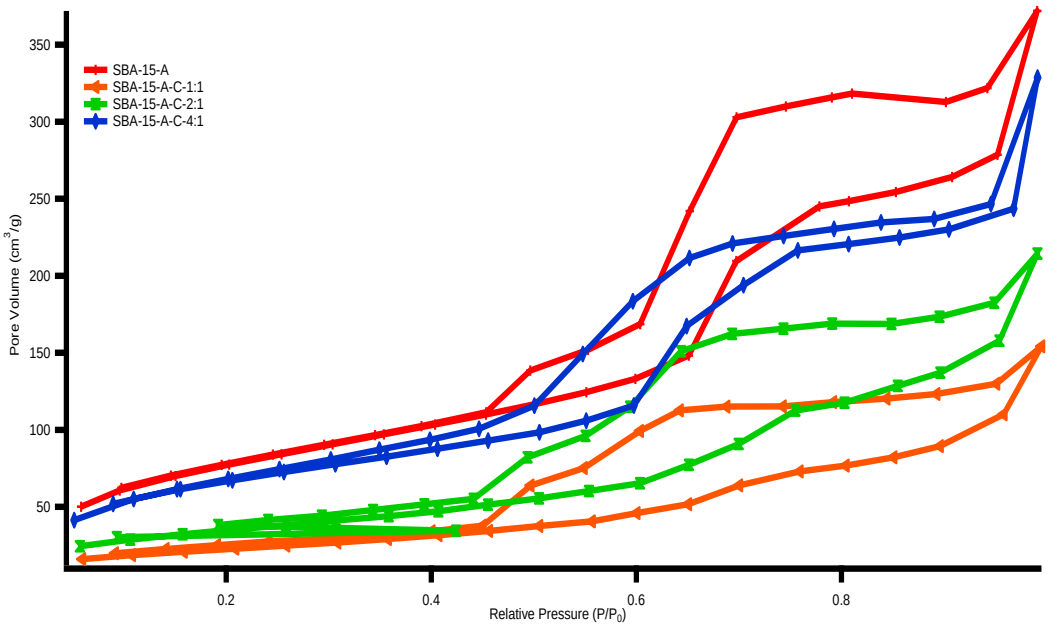

Figure-23: BET Isotherms of Pure and Celecoxib Loaded Amine Functionalized SBA-15 Particles.

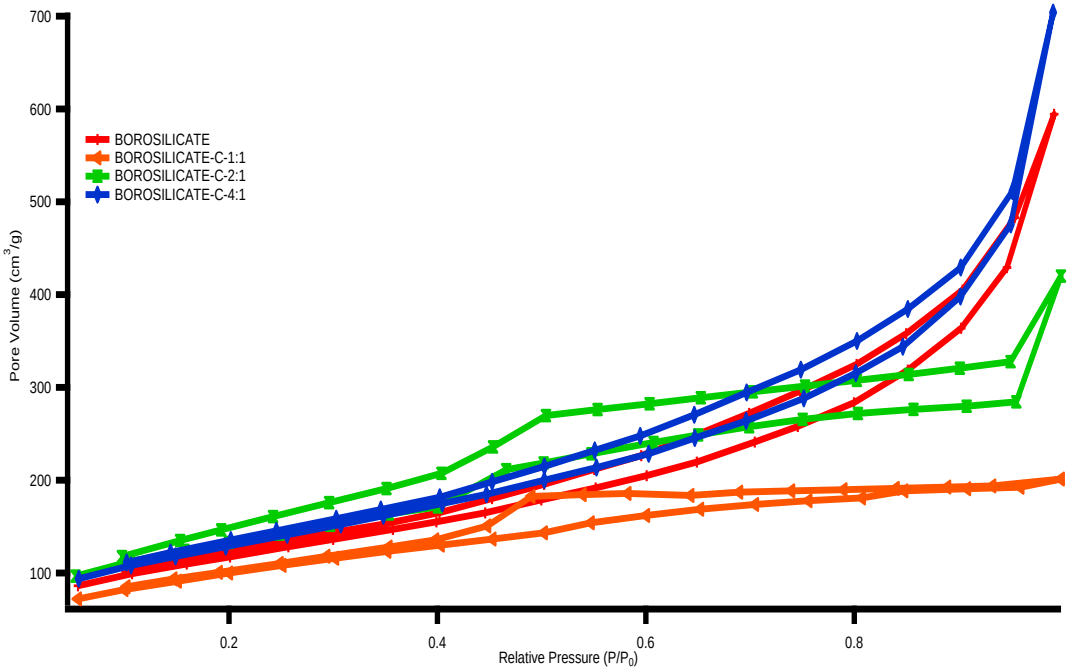

Figure-24: BET Isotherms of Pure and Celecoxib Loaded Borosilicate Particles.

The pore size, pore volume and surface area of pure and Celecoxib loaded SBA-15 and borosilicate samples are given in Table-4, Table-5 and Table-6.

Table-4: Pore Size Data of Pure and Celecoxib Loaded Samples.

Pore Size Data	**SBA-15**			**SBA-15-A**			**BOROSILICATE**		
BJH Method Adsorption Pore Diameter (nm)	6.824			6.539			2.211		
Pore Size Data	**PURE-C-1:1**	**PURE-C-2:1**	**PURE-C-4:1**	**A-C-1:1**	**A-C-2:1**	**A-C-4:1**	**BS-C-1:1**	**BS-C-2:1**	**BS-C-4:1**
BJH Method Adsorption Pore Diameter (nm)	5.647	6.563	6.54	6.570	5.665	5.601	1.943	3.485	2.756

The Table-4 illustrates the decrease in pore size data after Celecoxib loading except two of borosilicate samples. The pore size diameters were decreased due to Celecoxib loading of pores. However, increase in pore size diameter was observed of two borosilicate samples. This might be a consequence of poor absorption or connection of drugs with outer surface of pores. According to published article about borosilicate samples, only pure borosilicate sample's pore diameter is published and drug loaded sample's diameter values were not mentioned [37]. Besides, according to SAXS results, borosilicate samples do not have ordered pore structure and so, pore size diameter of borosilicate samples which were found in BJH method had some limitations.

Table-5: Pore Volume Data of Pure and Celecoxib Loaded Samples.

Pore Volume Data	**SBA-15**			**SBA-15-A**			**BOROSILICATE**		
BJH Method Cumulative Adsorption Pore Volume (cm^3/g)	1.119			0.6183			0.9265		
Pore Volume Data	**PURE-C-1:1**	**PURE-C-2:1**	**PURE-C-4:1**	**A-C-1:1**	**A-C-2:1**	**A-C-4:1**	**BS-C-1:1**	**BS-C-2:1**	**BS-C-4:1**
BJH Method Cumulative Adsorption Pore Volume (cm^3/g)	0.6484	2.195	0.9239	0.2467	0.3437	0.5510	0.3109	0.6554	1.104

The Table-5 shows that pore volume data of samples were decreased after Celecoxib loading. The reason of the reducing of the pore volume data of samples was the filling of pore channels with Celecoxib [29]. However, in some cases there was an increase in pore volume data and this might be caused by attachment of Celecoxib outer surface of samples.

Table-6: Surface Area Data of Pure and Celecoxib Loaded Samples.

Surface Area Data	**SBA-15**			**SBA-15-A**			**BOROSILICATE**		
Multipoint BET (m^2/g)	816.8			291.8			427.7		
Surface Area Data	**PURE-C-1:1**	**PURE-C-2:1**	**PURE-C-4:1**	**A-C-1:1**	**A-C-2:1**	**A-C-4:1**	**BS-C-1:1**	**BS-C-2:1**	**BS-C-4:1**
Multipoint BET (m^2/g)	365.1	501.3	716.3	84.23	129.3	253.2	365	477	474.8

The Table-6 demonstrates the reducing of surface area after Celecoxib loading. However, some of borosilicate samples had an increase of surface area data. This might be as a result of poor adsorption of Celecoxib or connection of inner surface.

To conclude, the pore size, pore volume and surface area values of samples were reduced after Celecoxib loading process. Generally, all samples had an expected result except borosilicate samples [38].

3.5.2. BJH METHOD

According to results, pure SBA-15 samples indicated pore size distribution in between 5.5-7.5 nm. After the Celecoxib loading samples showed quite same range of pore size.

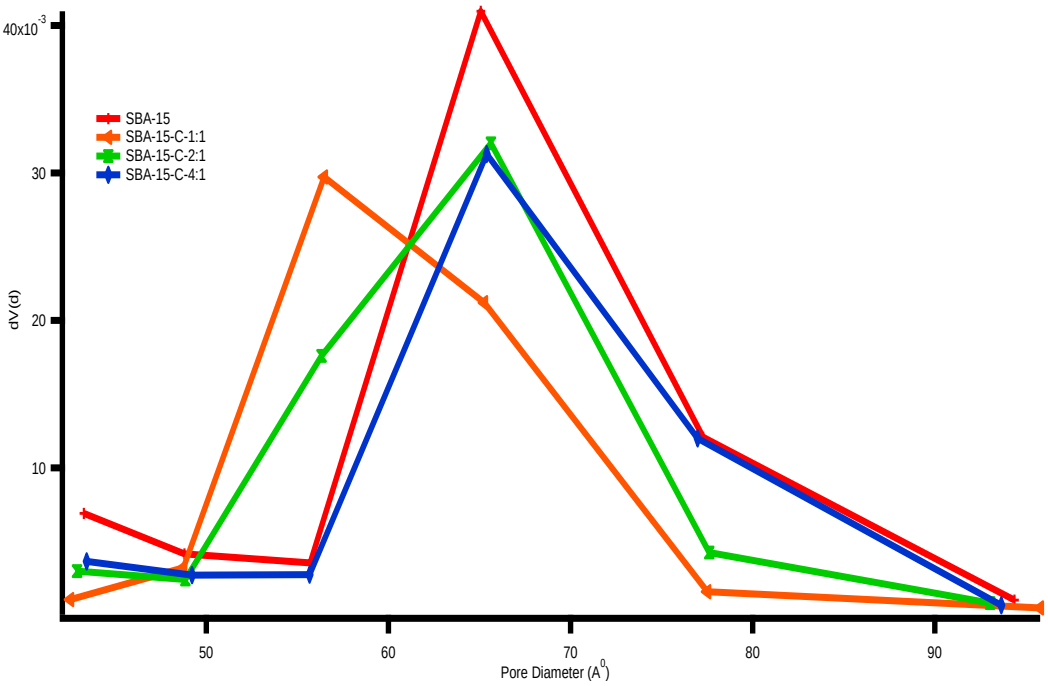

Figure-25: Pore Size Distribution of Pure and Celecoxib Loaded SBA-15 Samples.

Amine functionalized SBA-15 sample had a pore size distribution in the range of 5.0-8.0 nm. Celecoxib loaded samples had narrower pore size distribution.

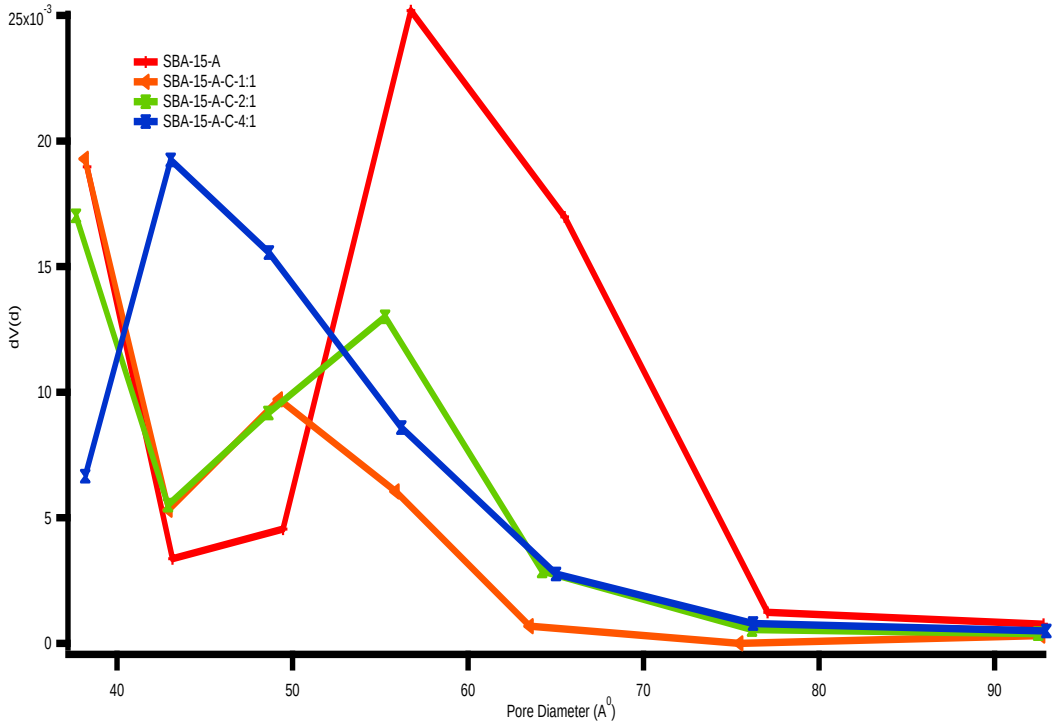

Figure-26: Pore Size Distribution of Pure and Celecoxib Loaded Amine Functionalized SBA-15 Samples.

Borosilicate samples have disordered mesopores because during the borosilicate synthesis aging process was not applied to improve ordering of pores. Therefore, in pore size measurements the regular pore size distributions were not obtained.

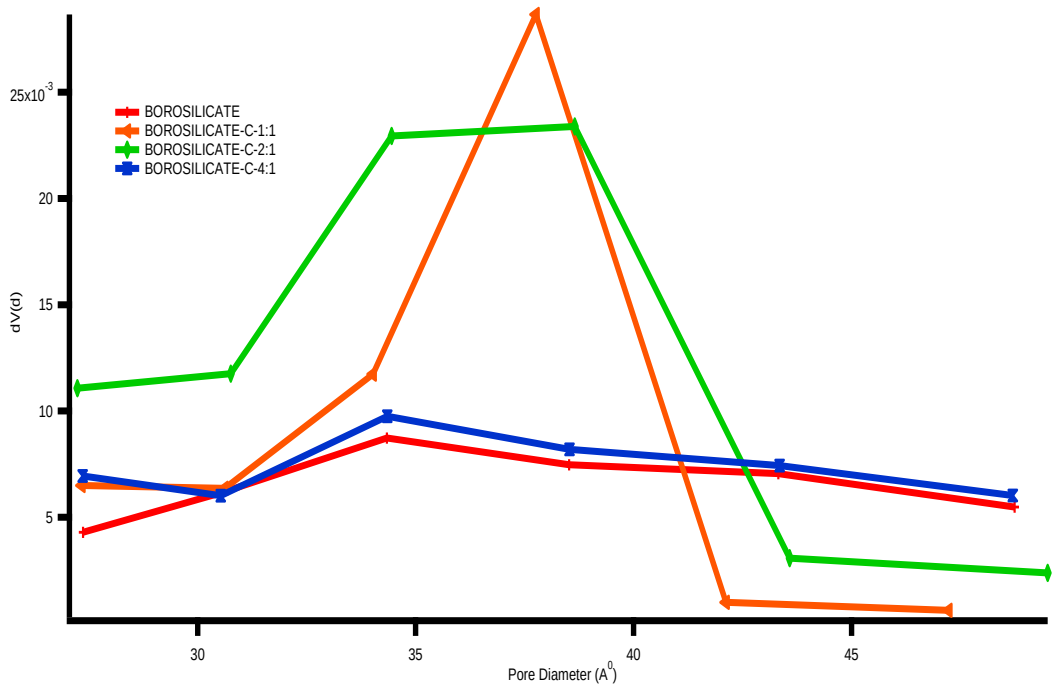

Figure-27: Pore Size Distribution of Pure and Celecoxib Loaded Borosilicate Samples.

3.6. TEM ANALYSIS

TEM images of samples exhibits that SBA-15 particles had hexagonal structure and well-defined mesopores. Amine functionalized SBA-15 samples also had highly-ordered mesoporous structure and so functionalized samples maintained their ordered and stable structure. However, borosilicate samples had disordered mesopores. This might be caused by boron incorporation. Therefore, boron doping reduced the ordered structure of silica materials [17, 37, 50]. TEM images of pure SBA-15, amine functionalized SBA-15 and borosilicate samples are given in Figure-28, Figure-29, Figure-30 respectively.

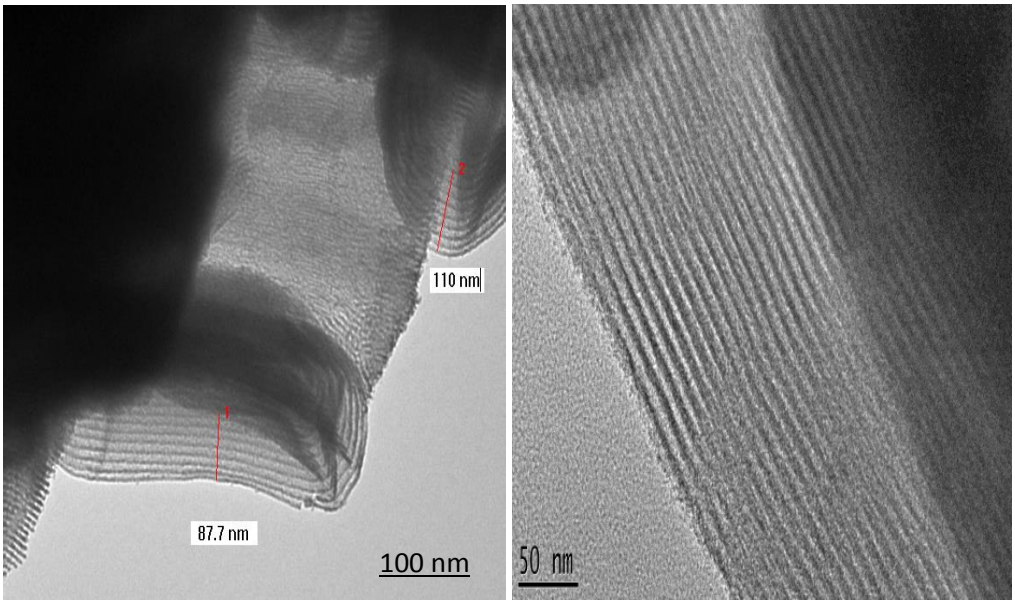

Figure-28: TEM Images of Pure SBA-15 Sample.

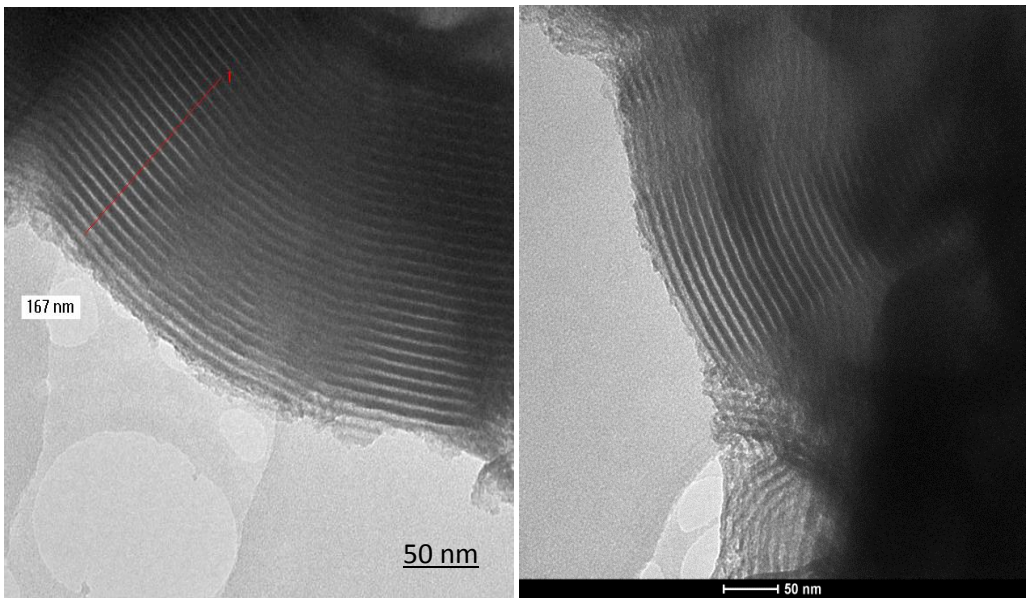

Figure-29: TEM Images of Amine Functionalized SBA-15 Sample.

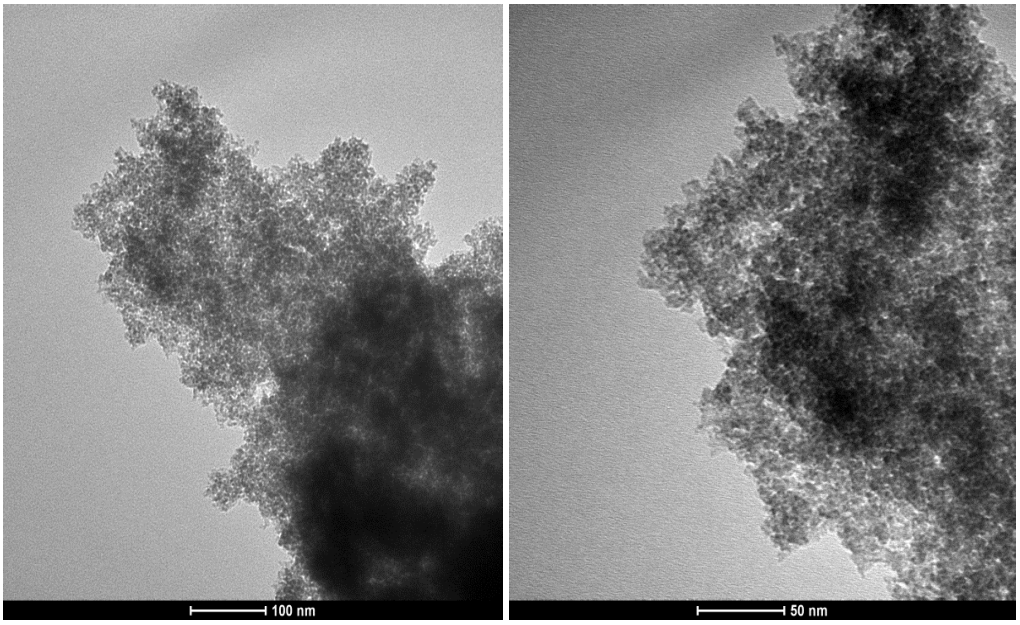

Figure-30: TEM Images of Borosilicate Sample.

TEM images of Celecoxib loaded pure SBA-15, amine functionalized SBA-15 and borosilicate samples are given in Figure-31, 32, 33, 34, 35, 36, 37, 38. According to TEM images of Celecoxib loaded samples, it is clear that all samples maintained their ordered and stable structure after drug loading process.

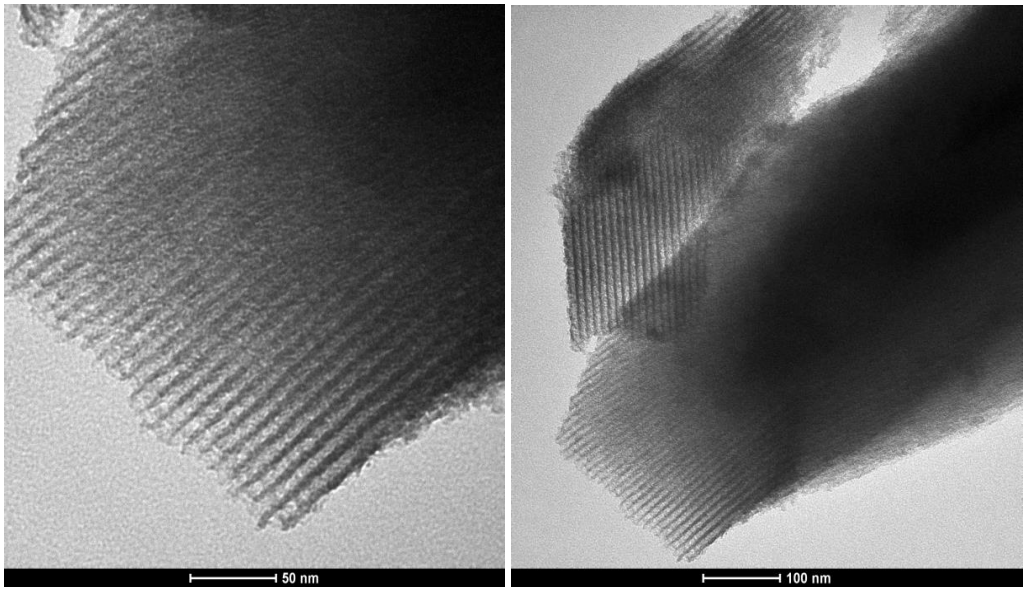

Figure-31: TEM Images of SBA-15+C 1:1 Sample.

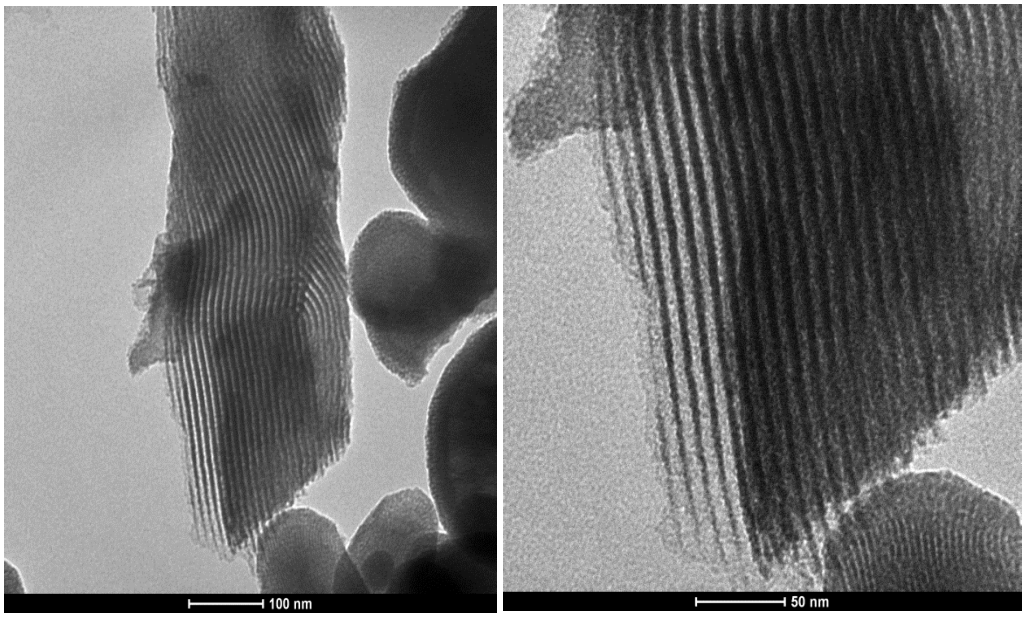

Figure-32: TEM Images of SBA-15+C 2:1 Sample.

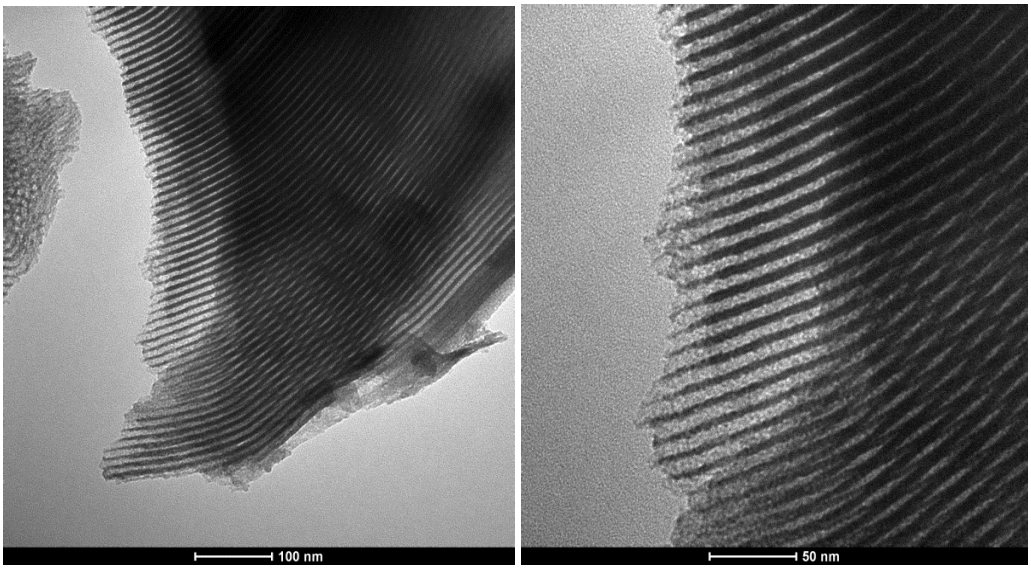

Figure-33: TEM Images of SBA-15+C 4:1 Sample.

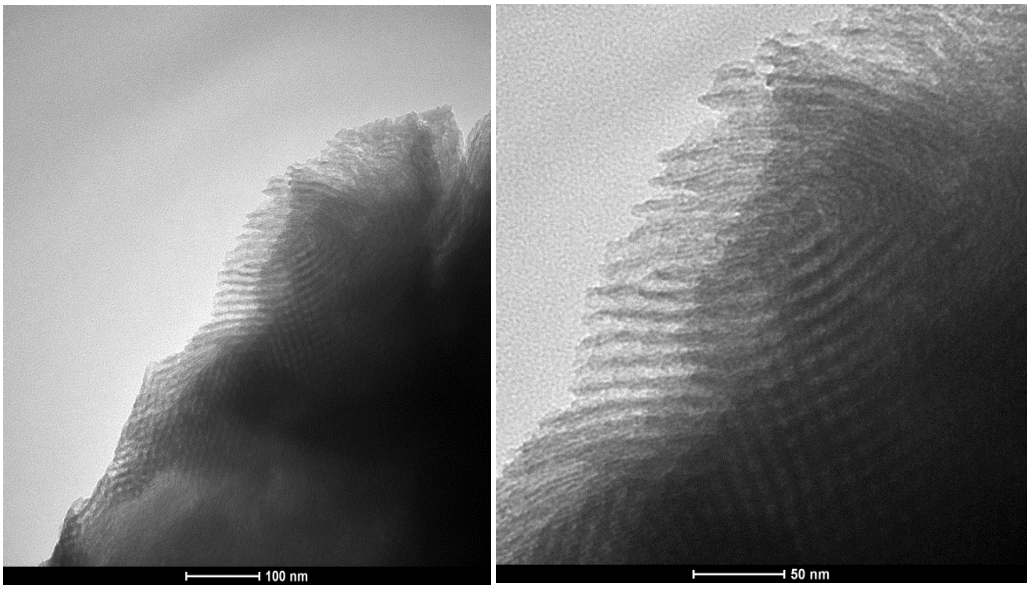

Figure-34: TEM Images of SBA-15+A+C 1:1 Sample.

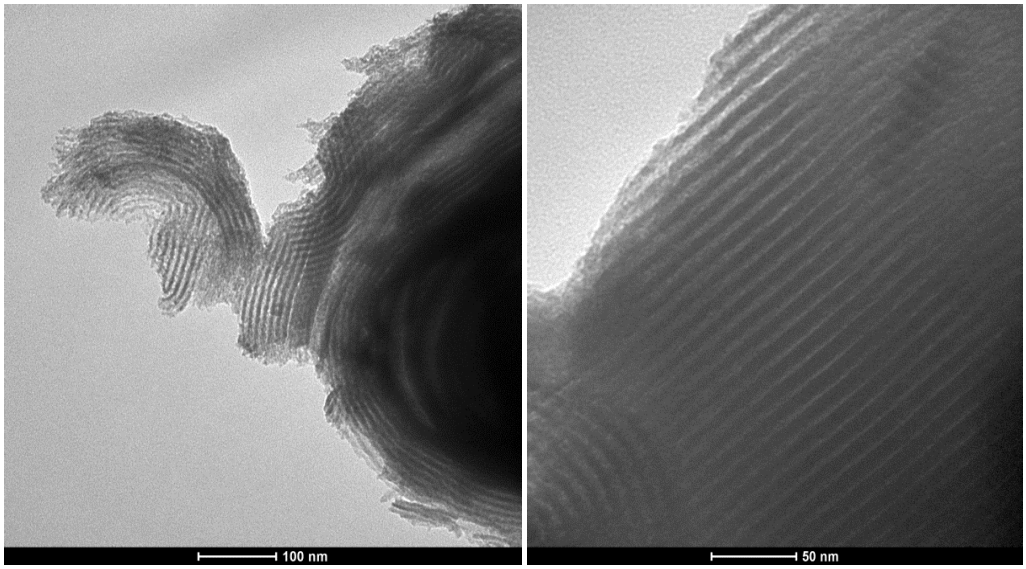

Figure-35: TEM Images of SBA-15+A+C 2:1 Sample.

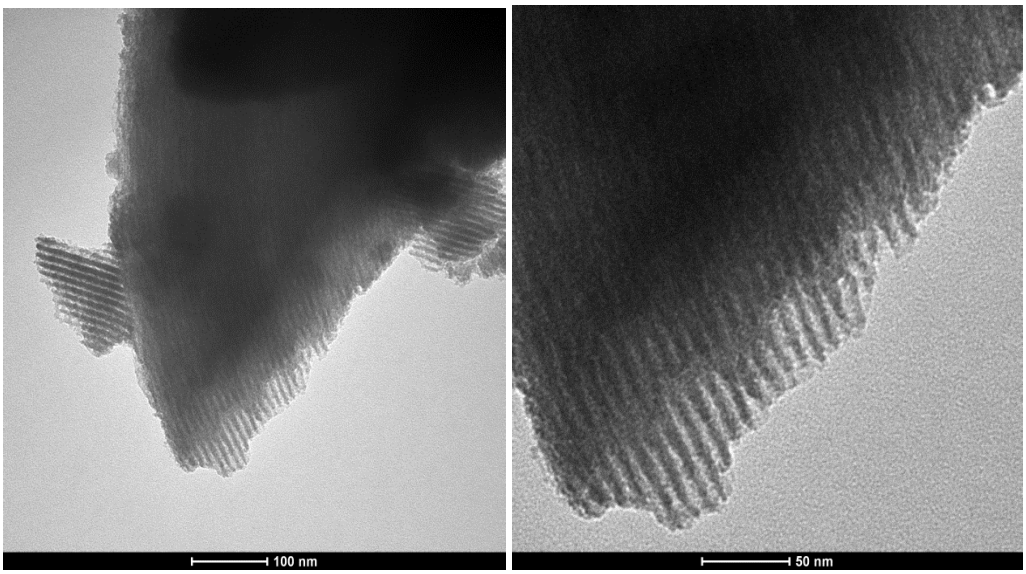

Figure-36: TEM Images of SBA-15+A+C 4:1 Sample.

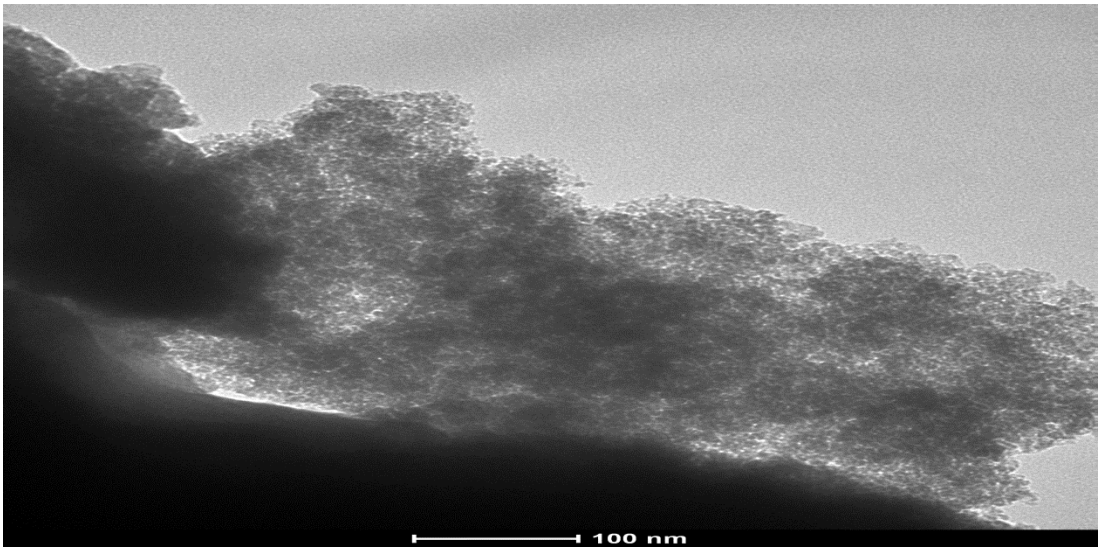

Figure-37: TEM Image of Borosilicate+C 1:1 Sample.

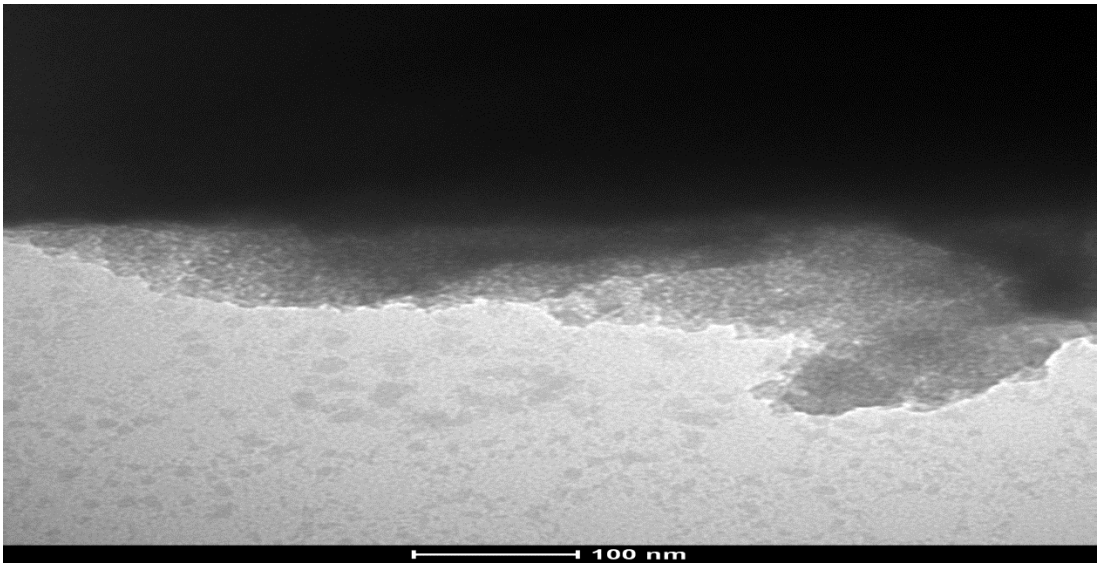

Figure-38: TEM Image of Borosilicate+C 2:1 Sample.

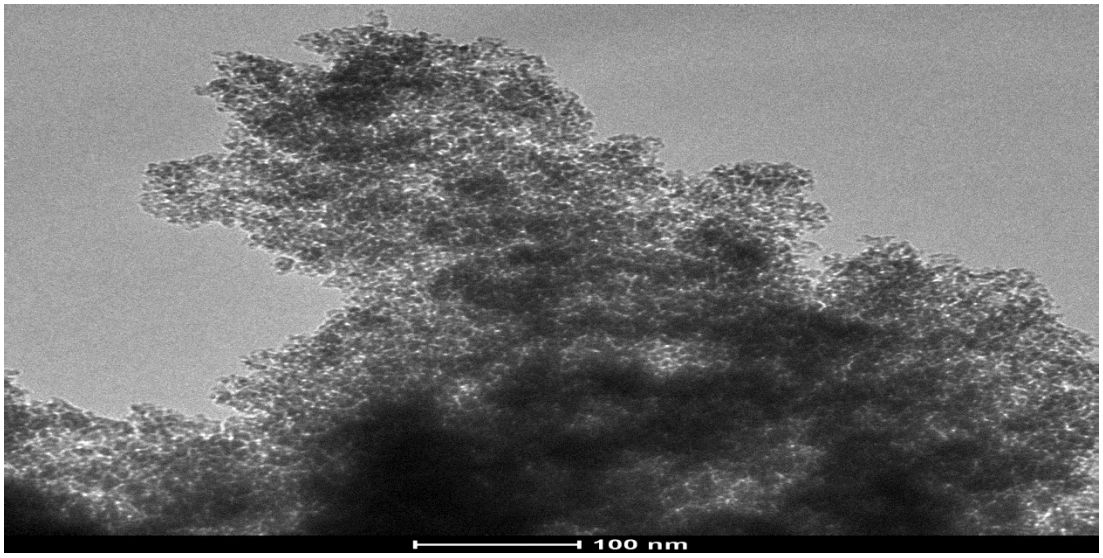

Figure-39: TEM Image of Borosilicate+C 4:1 Sample.

3.7. SEM ANALYSIS

SEM images of pure SBA-15, amine functionalized SBA-15, borosilicate samples and their Celecoxib loaded morphologies are given in Figure-40, 41, 42, 43, 44, 45, 44, 46, 47, 48, 49 and 50. According to SEM images; the pore system, hexagonally ordered structure and rodlike particles of SBA-15 samples were observed. After the functionalization and drug loading process, samples were maintaned their structral properties [51, 52]. Besides, borosilicate samples had tiny spherical units and aggregation of some of these nanoparticles. Also, borosilicate samples were preserved their structure after Celecoxib loading process [37].

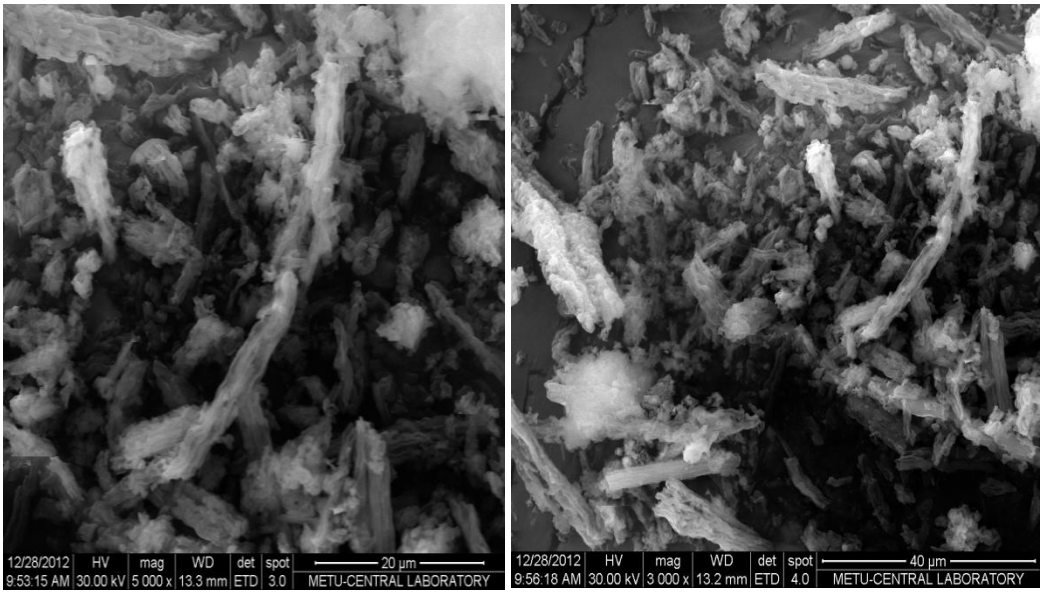

Figure-40: SEM Images of SBA-15 Sample.

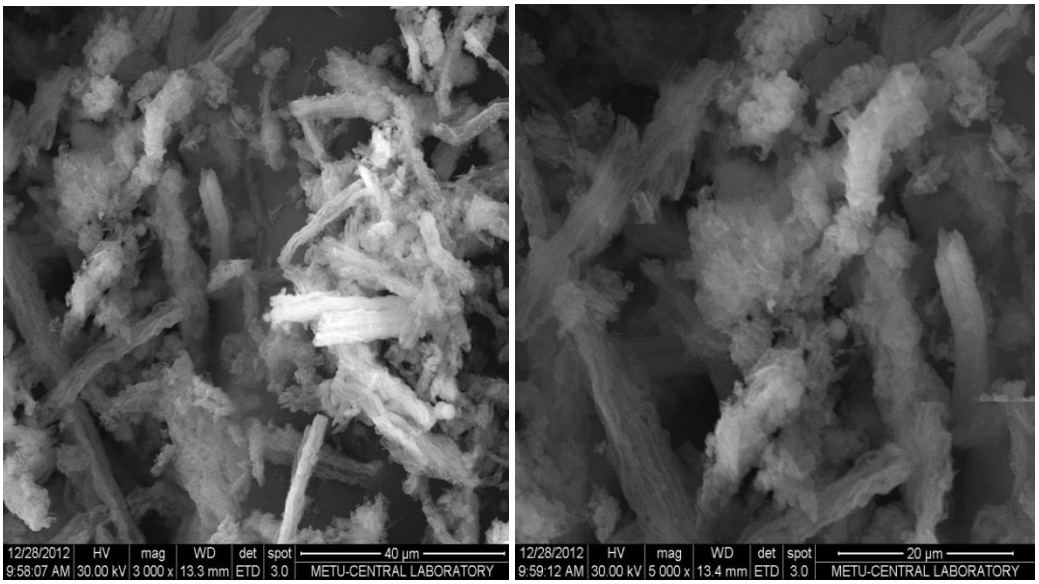

Figure-41: SEM Images of SBA-15+C 1:1 Sample.

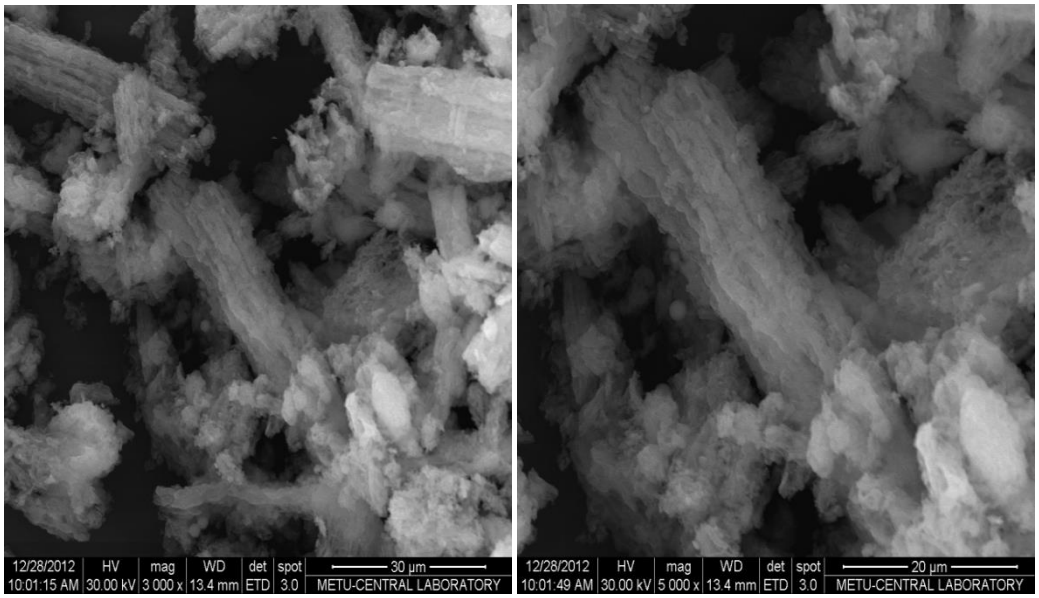

Figure-42: SEM Images of SBA-15+C 2:1 Sample.

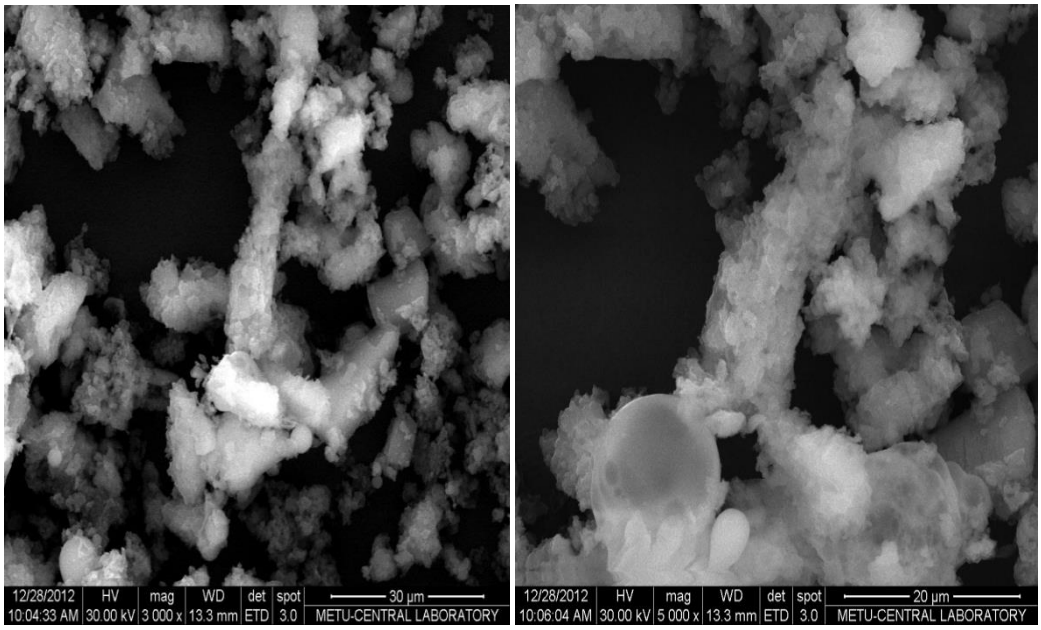

Figure-43: SEM Images of SBA-15+C 4:1 Sample.

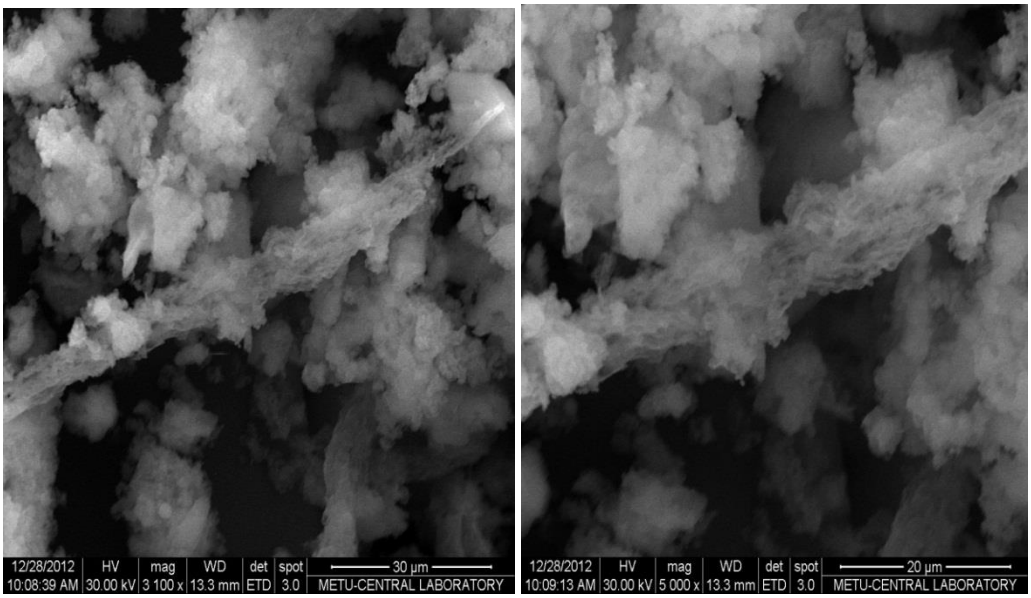

Figure-44: SEM Images of SBA-15+A Sample.

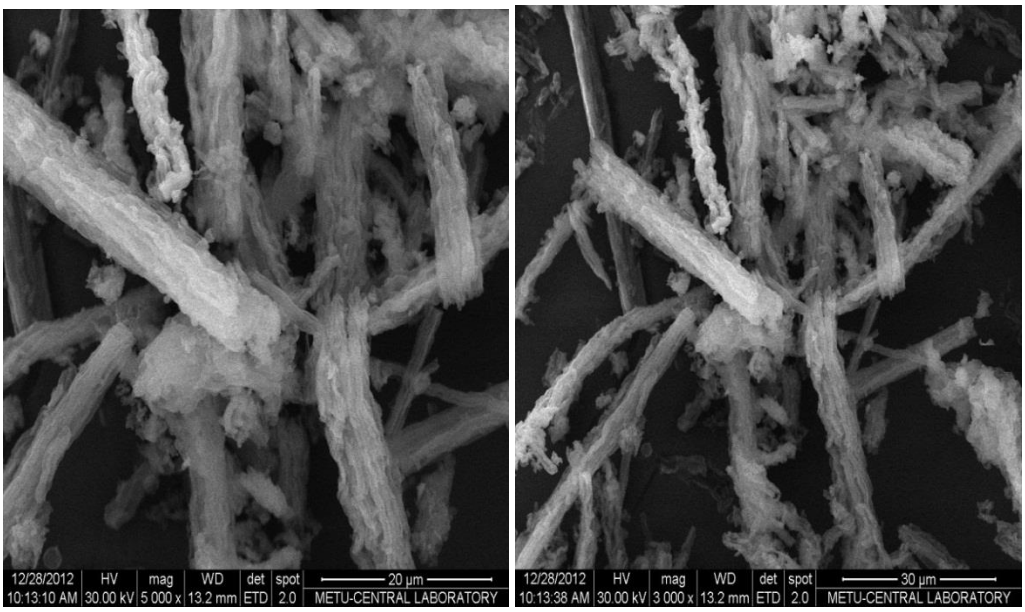

Figure-45: SEM Images of SBA-15+A+C 1:1 Sample.

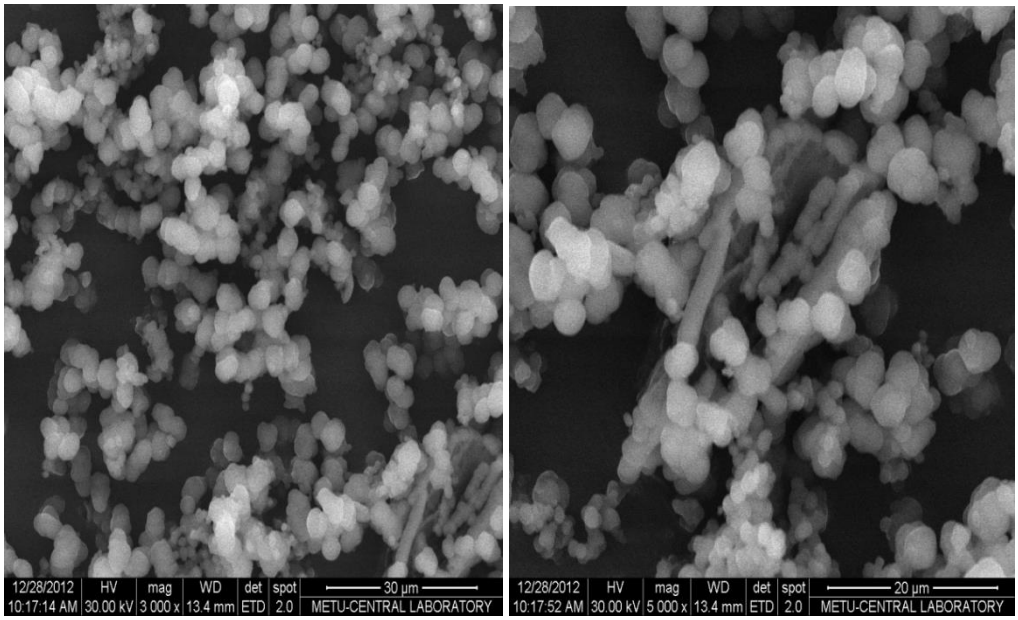

Figure-46: SEM Images of SBA-15+A+C 2:1 Sample.

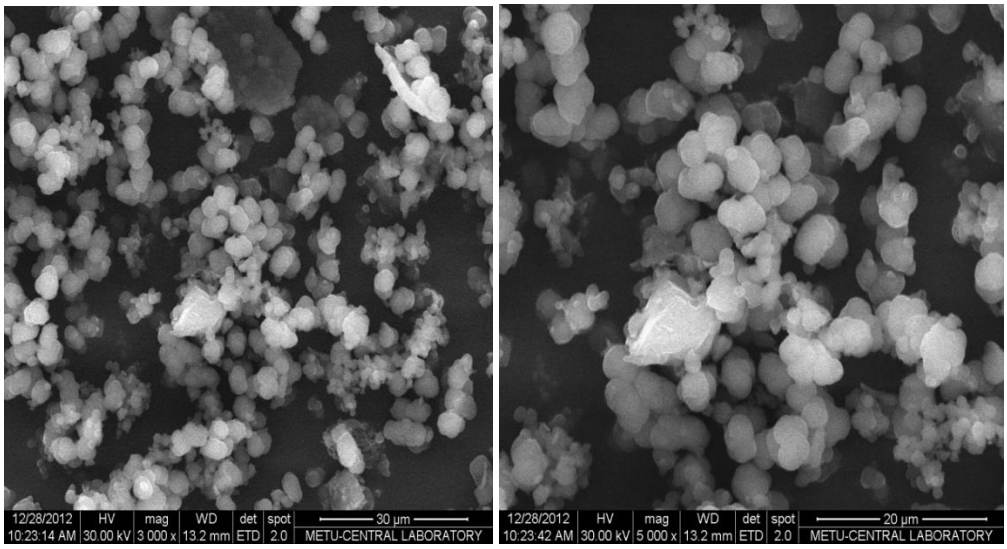

Figure-47: SEM Images of SBA-15+A+C 4:1 Sample.

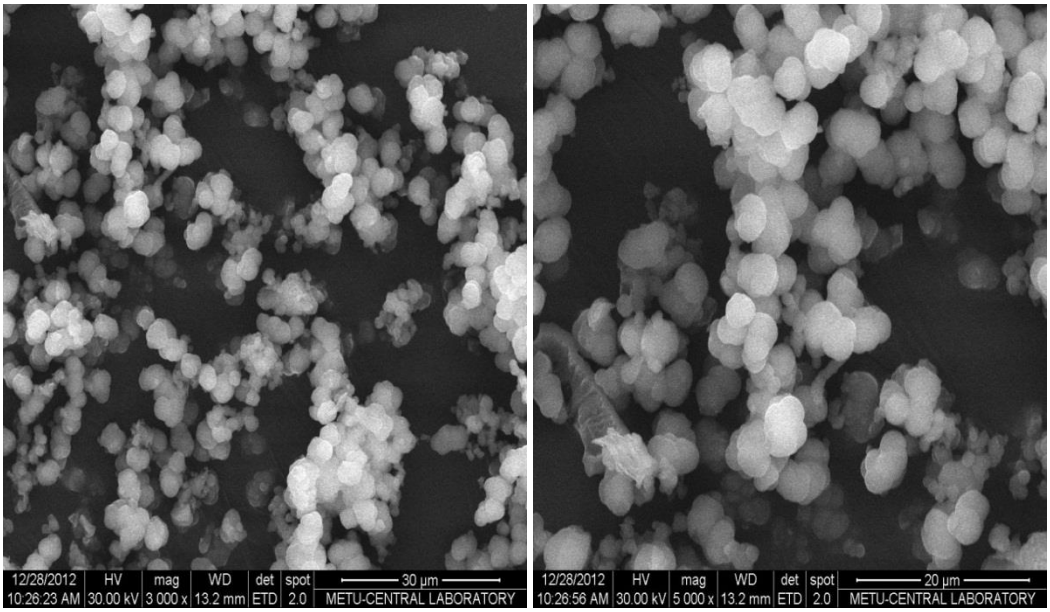

Figure-48: SEM Images of Borosilicate Sample.

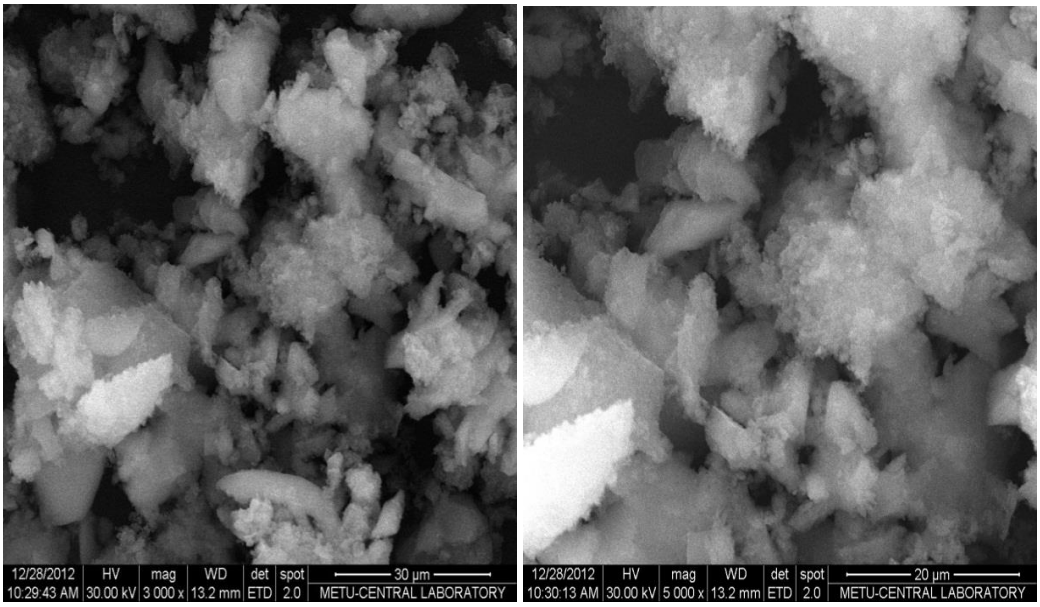

Figure-49: SEM Images of Borosilicate+C 1:1 Sample.

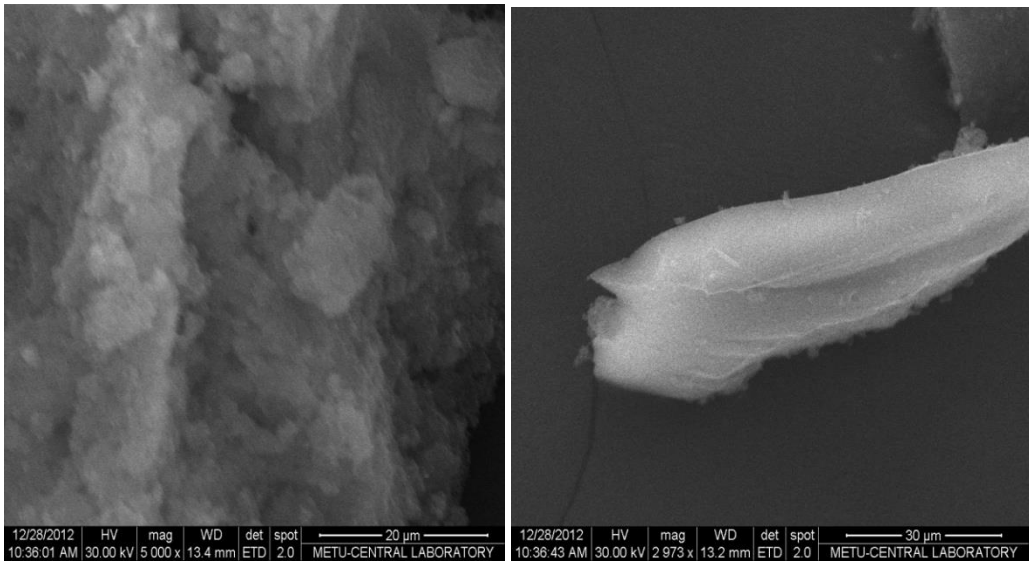

Figure-50: SEM Images of Borosilicate+C 2:1 Sample.

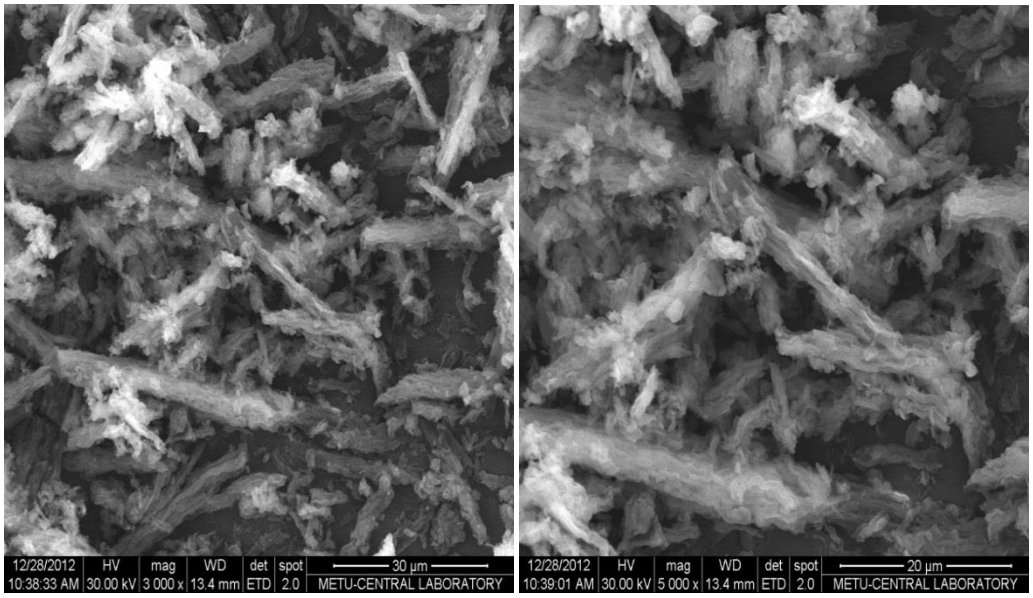

Figure-51: SEM Images of Borosilicate+C 4:1 Sample.

3.8. ZETA POTENTIAL MEASUREMENT

Zeta potential measurement gives information about surface properties of samples by using electric potential of surface. It gives information about electrical charge of the layer. Pure SBA-15 sample had quite neutral value at pH= 2 and negative zeta potential at other pH range due to negative charges of silanol groups. Borosilicate sample's surface also was highly negative and it had a negative value of zeta potential because of existence of hydroxyl groups on its surface. However, SBA-15+A sample had a more positive zeta potential values. Between the pH= 2 to 7, SBA-15+A samples had positive zeta potential value and after the pH= 7 this particle had negative zeta potential value. This might be caused by substitution of silanol groups with amine groups [53]. According to acid-base properties of the surface of the SBA-15, amine functionalized SBA-15 and Borosilicate samples, these equilibriums were suggested:

$-NH_2 + H_2O \longleftrightarrow -NH_3^+ + OH^-$

$-Si\text{-}OH + H_2O \longleftrightarrow -Si\text{-}O^- + H_3O^+$

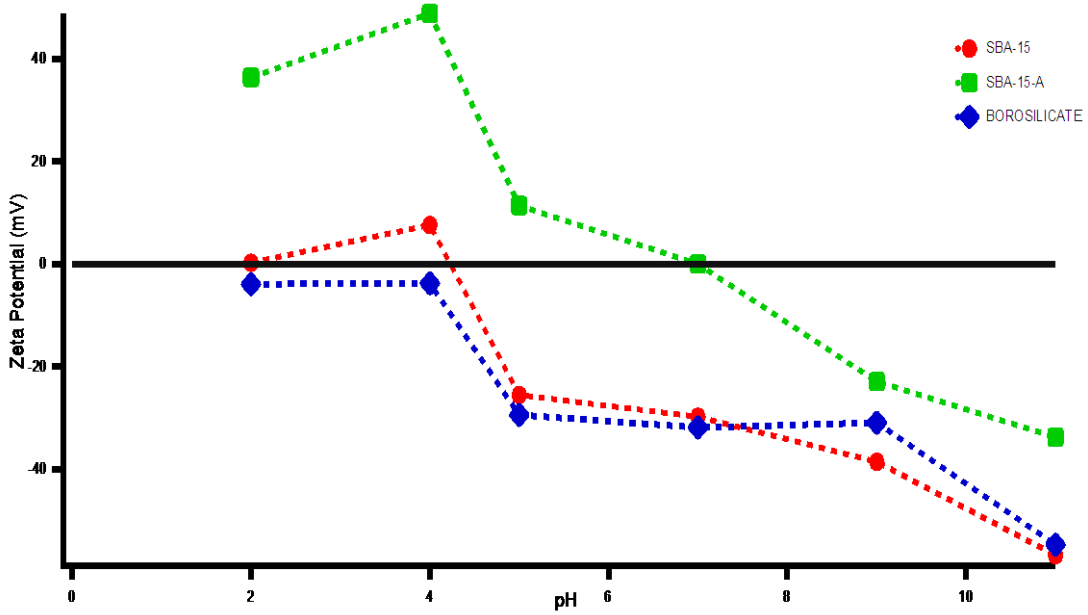

Figure-52: Zeta Potentials of Pure SBA-15, Amine Functionalized SBA-15 and Borosilicate Samples.

3.9. UV MEASUREMENTS

3.9.1. CELECOXIB LOADING

In order to do UV experiments standard solutions were prepared and used to plot of calibration curve. Solutions were prepared by dissolving of 0.01 g samples in 10 ml methanol and standard solutions were prepared in different concentrations that were 0.003125 M, 0.00625 M, 0.0125 M and 0.025 M. Then, the percentage of loaded Celecoxib was calculated by using Beer's Law (A=Ɛ.b.c). In this equation, molar absorptivity coefficient is equal to slope of calibration curve. Calibration curve's equation was obtained as $y = 3.4477x + 0.0902$ ($R^2 = 0.5443$).

Table-7: Absorbance Values of Celecoxib Loaded Pure SBA-15 Samples.

SBA-15+C 1:1		**SBA-15+C 2:1**		**SBA-15+C 4:1**	
Time (h)	**Absorbance**	**Time (h)**	**Absorbance**	**Time (h)**	**Absorbance**
0	0	0	0	0	0
4	0.232	4	0.299	4	0.283
8	0.246	8	0.284	8	0.291
24	0.277	24	0.351	24	0.366
32	0.188	32	0.372	32	0.298
48	0.358	48	0.363	48	0.392

Table-8: Absorbance Values of Celecoxib Loaded Amine Functionalized SBA-15 Samples.

SBA-15+A+C 1:1		SBA-15+A+C 2:1		SBA-15+A+C 4:1	
Time (h)	**Absorbance**	**Time (h)**	**Absorbance**	**Time (h)**	**Absorbance**
0	0	0	0	0	0
4	0.298	4	0.332	4	0.373
8	0.291	8	0.309	8	0.321
24	0.361	24	0.297	24	0.351
32	0.242	32	0.333	32	0.353
48	0.398	48	0.385	48	0.411

Table-9: Absorbance Values of Celecoxib Loaded Borosilicate Samples.

Borosilicate+C 1:1		Borosilicate+C 2:1		Borosilicate+C 4:1	
Time (h)	**Absorbance**	**Time (h)**	**Absorbance**	**Time (h)**	**Absorbance**
0	0	0	0	0	0
4	0.277	4	0.328	4	0.323
8	0.293	8	0.335	8	0.360
24	0.193	24	0.279	24	0.481
32	0.291	32	0.407	32	0.505
48	0.305	48	0.671	48	0.575

Table-10: % Loaded Celecoxib of Pure SBA-15, Amine Functionalized SBA-15 and Borosilicate Samples.

Sample	**SBA-15+C 1:1**	**SBA-15+C 2:1**	**SBA-15+C 4:1**
%Loaded Celecoxib	24.63	36.05	58.46
Sample	**SBA-15+A+C 1:1**	**SBA-15+A+C 2:1**	**SBA-15+A+C 4:1**
%Loaded Celecoxib	29.83	34.85	61.72
Sample	**Borosilicate+C 1:1**	**Borosilicate+C 2:1**	**Borosilicate+C 4:1**
%Loaded Celecoxib	25.80	46.90	76.33

According to results, in all type of samples, highest efficiency of drug loading achieved by the silica: Celecoxib ratio of 4:1by weight. While preparing precursor solution with same weight of silica and Celecoxib the lowest efficiency of loading obtained. The reason of the effect of different concentration of drug in solution to loading efficiency may be related with the mobility's of molecules in aqueous media: In highly concentrated solution Celecoxib molecules have lower possibility to interact with the functional groups available on the silica surface. Another reason may be the functionalization of the surface of silica is limited to make interaction with drug molecules. Highest drug loading measured in borosilicate sample with 4:1 weight ratio of silica and drug, means that there were more hydroxyl groups on the surface to create strong interaction with Celecoxib and borsilicate surface. Celecoxib loaded graphs of samples are given in Figure-53, Figure-54 and Figure-55.

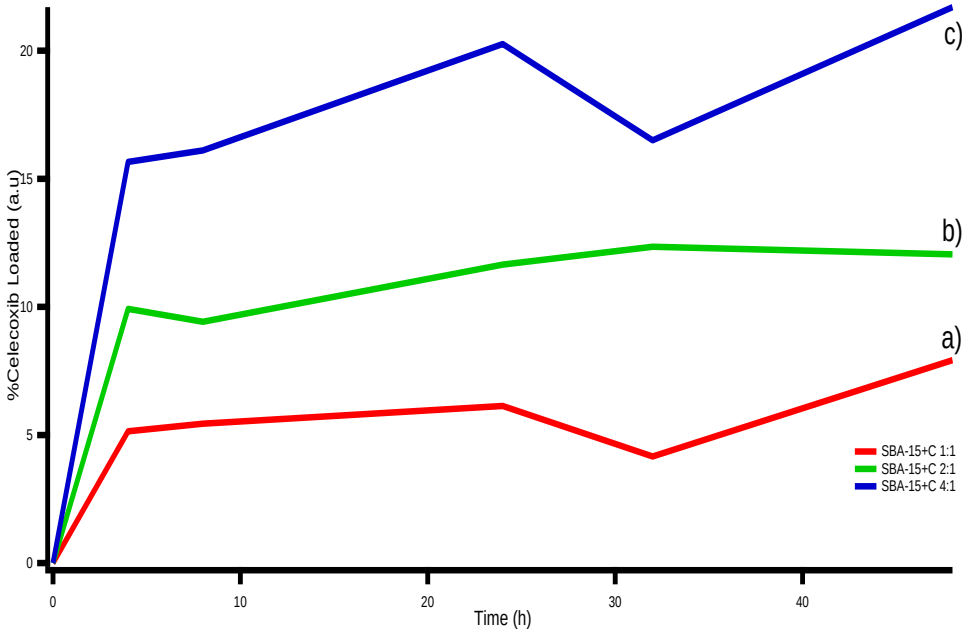

Figure-53: Graph of Celecoxib Loaded Pure SBA-15 Samples. a) SBA-15+C 1:1, b) SBA-15+C 2:1, c) SBA-15+C 4:1

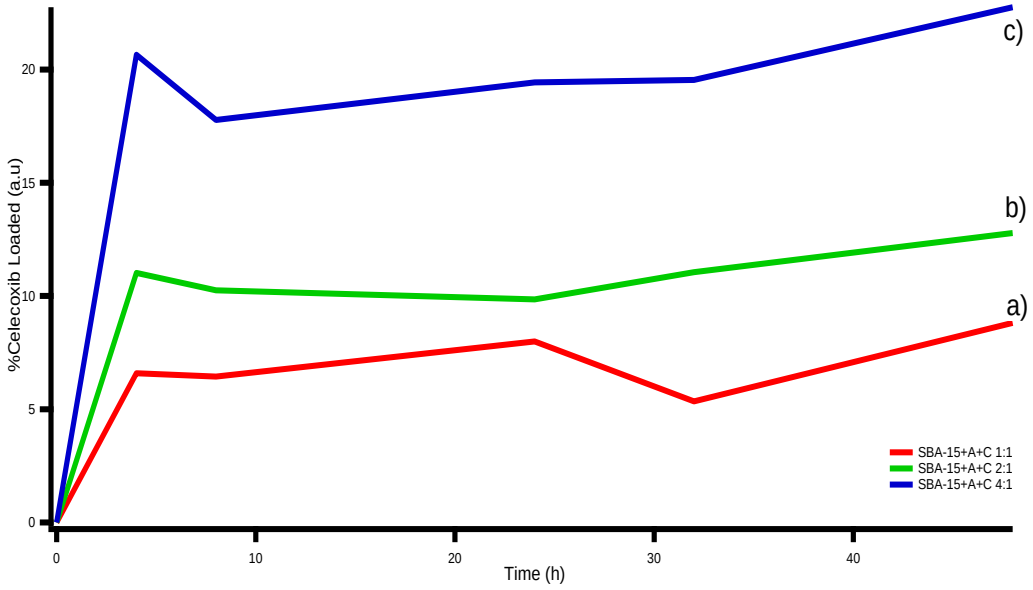

Figure-54: Graph of Celecoxib Loaded Amine Functionalized SBA-15 Samples. a) SBA-15+A+C 1:1, b) SBA-15+A+C 2:1, c) SBA-15+A+C 4:1

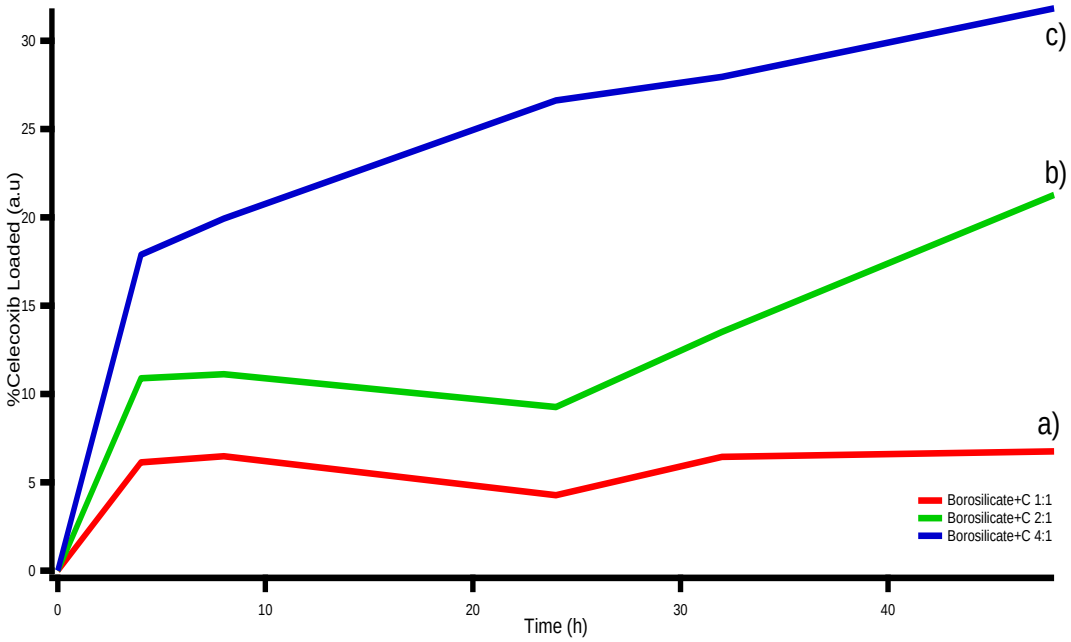

Figure-55: Graph of Celecoxib Loaded Borosilicate Samples. a) Borosilicate+C 1:1, b) Borosilicate+C 2:1, c) Borosilicate+C 4:1

3.9.2. CELECOXIB RELEASE

Release experiment was done as a same method with loading process instead of methanol. Standard solutions were prepared with different concentrations that were 0.003125 M, 0.00625 M, 0.0125 M and 0.025 M. Then, calibration curve was obtained and calibration curve's equation was equal to $y = 7.596x - 0.0127$ ($R^2 = 0.9784$). In order to calculate % amount of released Celecoxib Beer's Law equation was used.

Table-11: Absorbance Values of Celecoxib Released Pure SBA-15 Samples.

SBA-15+C 1:1		SBA-15+C 2:1		SBA-15+C 4:1	
Time (min)	**Absorbance**	**Time (min)**	**Absorbance**	**Time (min)**	**Absorbance**
0	0	0	0	0	0
30	0.337	30	0.274	30	0.314
60	0.294	60	0.148	60	0.284
120	0.313	120	0.282	120	0.272
240	0.282	240	0.271	240	0.253
360	0.251	360	0.260	360	0.284

Table-12: Absorbance Values of Celecoxib Released Amine Functionalized SBA-15 Samples.

SBA-15+A+C 1:1		SBA-15+A+C 2:1		SBA-15+A+C 4:1	
Time (min)	**Absorbance**	**Time (min)**	**Absorbance**	**Time (min)**	**Absorbance**
0	0	0	0	0	0
30	0.338	30	0.285	30	0.281
60	0.304	60	0.323	60	0.370
120	0.255	120	0.268	120	0.361
240	0.266	240	0.269	240	0.335
360	0.276	360	0.270	360	0.309

Table-13: Absorbance Values of Celecoxib Released Borosilicate Samples.

Borosilicate+C 1:1		Borosilicate+C 2:1		Borosilicate+C 4:1	
Time (min)	**Absorbance**	**Time (min)**	**Absorbance**	**Time (min)**	**Absorbance**
0	0	0	0	0	0
30	0.275	30	0.286	30	0.281
60	0.298	60	0.273	60	0.328
120	0.284	120	0.289	120	0.299
240	0.298	240	0.281	240	0.296
360	0.321	360	0.168	360	0.292

Table-14: % Released Celecoxib of Pure SBA-15, Amine Functionalized SBA-15 and Borosilicate Samples.

Sample	**SBA-15+C 1:1**	**SBA-15+C 2:1**	**SBA-15+C 4:1**
%Released Celecoxib	14.85	18.61	33.09
Sample	**SBA-15+A+C 1:1**	**SBA-15+A+C 2:1**	**SBA-15+A+C 4:1**
%Released Celecoxib	14.47	21.32	41.61
Sample	**Borosilicate+C 1:1**	**Borosilicate+C 2:1**	**Borosilicate+C 4:1**
%Released Celecoxib	14.88	19.55	37.57

According to results, SBA-15+A+C 4:1 and Borosilicate+C 4:1 had the best release rates because they had the best release percentage of Celecoxib. Loading capacity of SBA-15++C 4:1 and Borosilicate+C 4:1 also showed best results. Besides; Figure-54, Figure-55 and Figure-56 indicate that release of Celecoxib could be controlled by using SBA-15and borosilicate samples as a drug delivery systems.

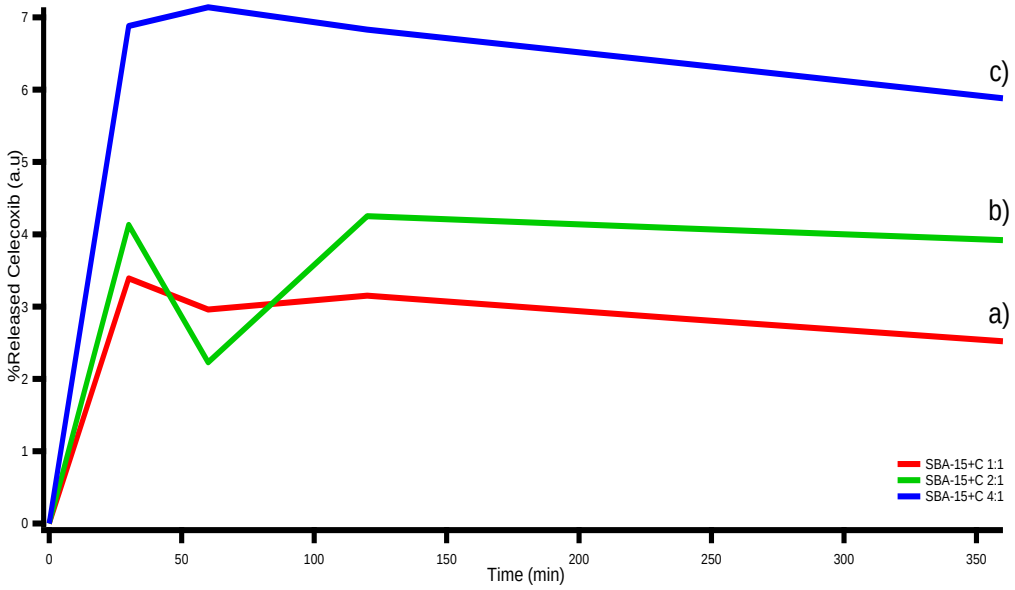

Figure-56: Graph of Celecoxib Released Pure SBA-15 Samples. a) SBA-15+C 1:1, b) SBA-15+C 2:1, c) SBA-15+C 4:1

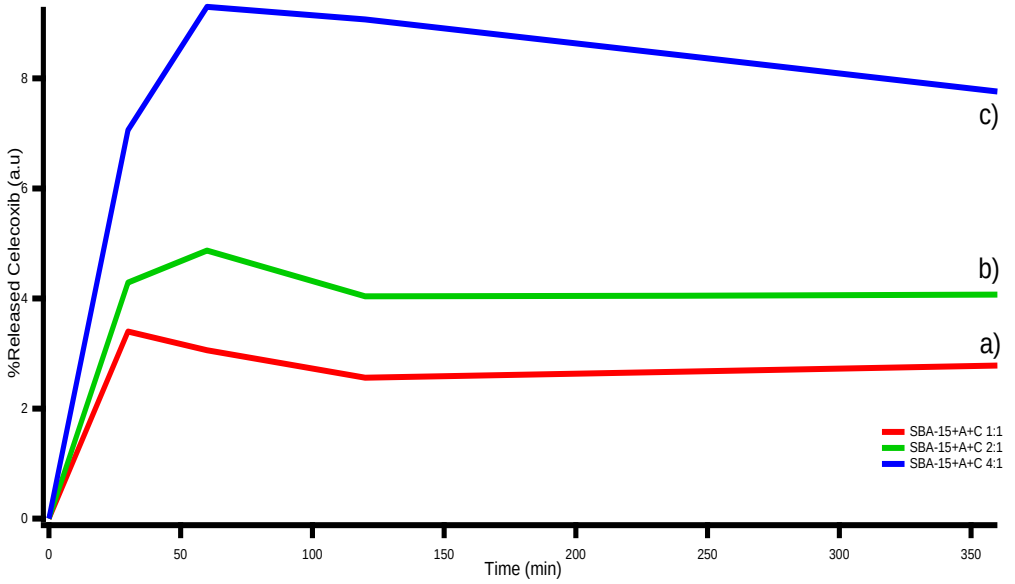

Figure-57: Graph of Celecoxib Released Amine Functionalized SBA-15 Samples. a) SBA-15+A+C 1:1, b) SBA-15+A+C 2:1, c) SBA-15+A+C 4:

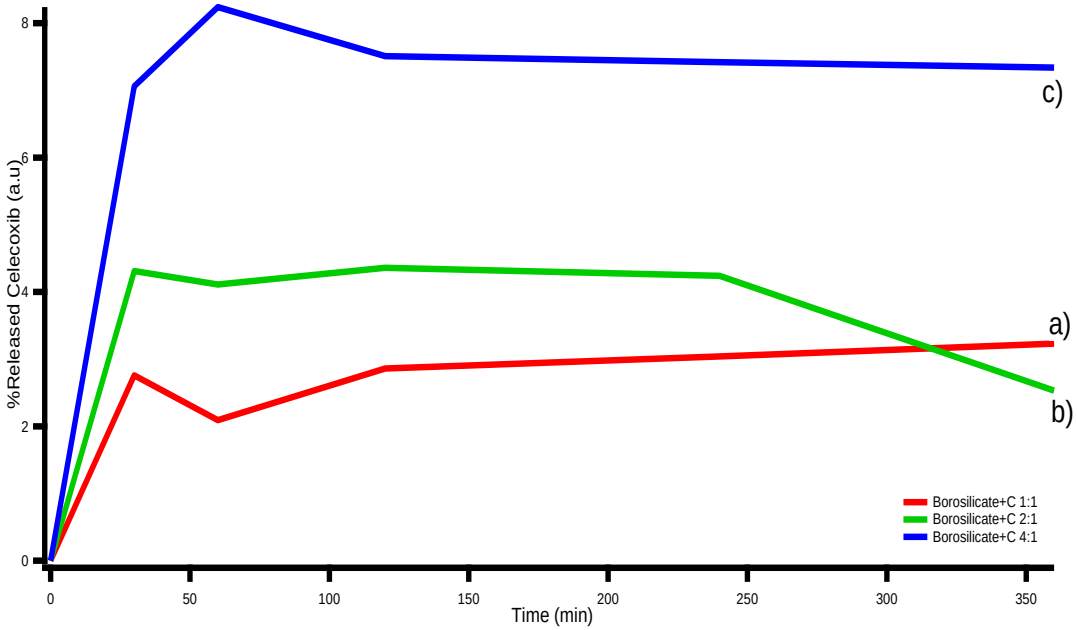

Figure-58: Graph of Celecoxib Released Borosilicate Samples. a) Borosilicate+C 1:1, b) Borosilicate+C 2:1, c) Borosilicate+C 4:1

3.10. HPLC ANALYSIS

HPLC analysis was done for only all borosilicate samples and 4:1 (sample/drug) ratio of SBA-15 samples. By using HPLC method the best release rates were obtained for SBA-15+A+C 4:1 and Borosilicate+C 4:1 sample as a 41.00 % and 30.27 % respectively. % Release rate of Celecoxib of samples are given in Figure-59. These results had some differences from UV analysis due to instrumental differences. In HPLC experiments, column was used and this might be more efficient way small amount of drug release. However, release rate of pure Celecoxib was obtained 26.00 % in HPLC experiment and this shows that amine functionalized SBA-15 and borosilicate samples had more efficient release rates. Release of Celecoxib could be maintained by using SBA-15 and borosilicate samples as controlled drug delivery systems.

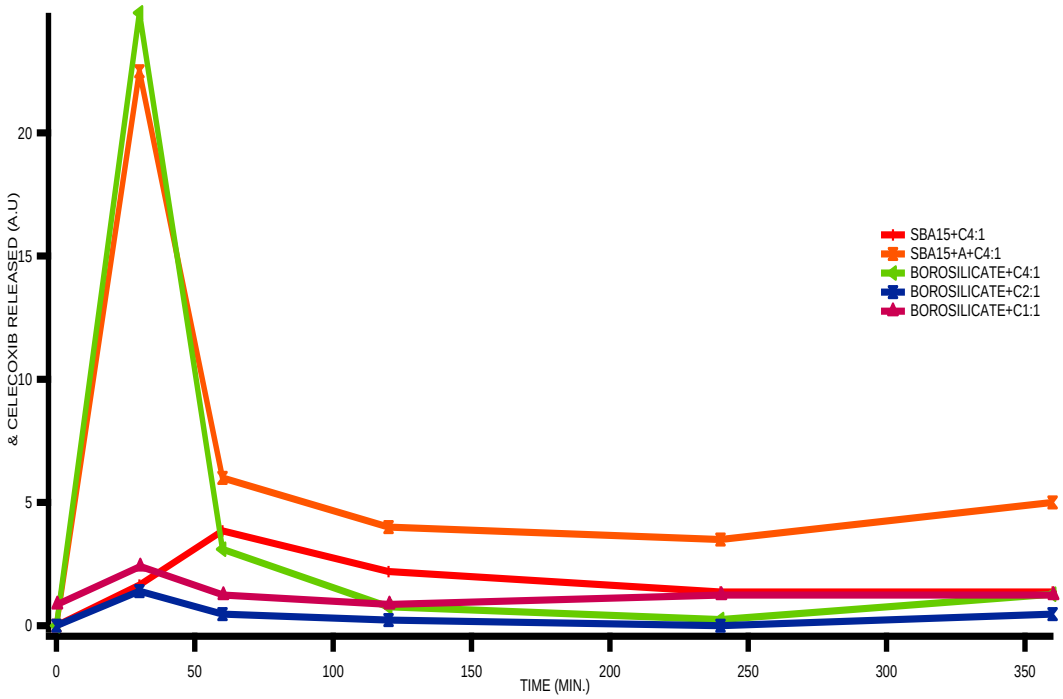

Figure-59: Graph of Celecoxib Release of SBA-15 and Borosilicate Samples Measured by HPLC.

CHAPTER 4

CONCLUSION

In order to enhance drug delivery, SBA-15mesoporous silica surface were functionalized with amine group and borosilicate samples were prepared. Characterization of samples were applied both pure, functionalized and Celecoxib loaded silica samples.

Elemental analysis was done to control the percent efficiency of drug loading process. Besides, loading capacity of drugs was controlled by using UV spectrometry. According to results SBA-15+A+C 4:1 and Borosilicate+C 4:1 had the best drug loading capacities which were 61.72 % and 76.33 % respectively. These results showed that functionalization process helps to enhance drug loading capacity.

By using powder X-Ray diffraction method, the order of pores of samples was determined as hexagonal unit cell (P6mm) 2D structure. XRD method was not the good way to observe highest intensity diffraction peaks (1 0 0). Therefore, SAXS analysis was done. In the SAXS analysis, 3 diffraction peaks (1 0 0), (1 1 0) and (2 0 0) of most samples were obtained. Moreover, most intense (1 0 0) diffraction peaks were obtained in all samples. After the Celecoxib loading ordered structure of samples were maintained and this showed that samples were ordered and stable. Besides, d-spacing values of samples were calculated by using SAXS analysis. These values were also in accordance with the data in literature.

The FTIR spectra of all samples were quite same except some differences. There was a difference at 3000-3500 cm^{-1} and this might be linkage of drugs and SBA-15 and borosilicate samples. Additionally, small peaks were observed about 3300-3400 cm^{-1} compared with pure samples and this might be caused by Celecoxib loading.

In order to analyze pore size distribution, pore volume distribution and surface area of particles N_2 adsorption-desorption method was used. Pore size distribution of samples quite same after Celecoxib loading process. As a result; pore size, pore volume and surface area of samples were decreased after Celecoxib loading.

TEM and SEM analysis of samples gave information about their structure. Both method showed that SBA-15 samples had hexagonally ordered mesoporous structure. Besides, these samples had rod like structure and ordered porous. Borosilicate samples showed spherical, porous structure. After Celecoxib loading process, it was observed that all samples prevented their ordered, porous structures.

In order to do surface analysis zeta potential measurement was conducted. According to zeta potential results, SBA-15 and borosilicate samples gave more negative values than SBA-15+A

sample. This might be caused by silanol and hydroxyl groups in SBA-15 and borosilicate samples. Due to amine groups of SBA-15+A sample had a more positive zeta potential value.

UV spectrometry and HPLC were used to control release rate of Celecoxib. The percentages of release rate of Celecoxib were calculated by using these two methods. As a result, controlled drug release was obtained for all samples and Borosilicate+C 4:1 and SBA-15+A+C samples had highest release rate of Celecoxib which were 37.57 % and 41.61 % respectively.

In conclusion, loading capacity and release rate of Celecoxib are changeable according to concentration of Celecoxib and functionalization type. However, it is clear that surface functionalization is a good method to enhance drug loading capacity.

REFERENCES

1) U. Ciesla, F. Schuth. (1998). *Microporous and Mesoporous Materials,* 27, 131-149.

2) C.T. Kresge, M.E. Leonowicz, W. J. Roth, W. J. Vartuli, J.S. Beck. (1992). *Nature*, 359, 710-712.

3) M. Vallet-Regi, F. Balas, D. Arcos. (2007). *Angew. Chem. Int. Ed.*, 46, 7548-7558.

4) M. Vallet-Regi, A. Ramila, R. P. del Real, J. Perez-Pariente. (2001). *Chem. Mater*, 13, 308-311.

5) V. Meynen, P. Cool, E.F. Vansant. (2009). *Microporous and Mesoporous Materials,* 125, 170-223.

6) J.S. Beck, J.C. Vartuli, W. J. Roth, M.E. Leonowicz, C.T. Kresge, K.D. Schmitt, C.T-W. Chu, D.H. Olson, E. W. Sheppard, S.B. McCullen, J.B. Higgins, J. L. Schlenkert. (1992). *J. Am. Chem. Soc.*, 114, 10834-10843.

7) A. Katiyar, S. Yadav, P. G. Smirniotis, N. G. Pinto. (2006). *Journal of Chromatography A,* 1122, 13-20.

8) T.-L. Chew, A. L. Ahmad, S. Bhatia. (2010). *Advances in Colloid and Interface Science*, 153, 43-57.

9) W.-H. Zhang, J. Lu, B. Han, M. Li, J. Xiu, P. Ying, C. Li. (2002). *Chem. Mater.* , 14, 3413-3421.

10) S. Wang. (2009). *Microporous and Mesaporous Materials*, 117, 1-9

11) S. Inagaki, Y. Fukushima, K. Kuroda. (1993). *J. Chem. Soc., Chem. Commun.*, 680-682.

12) Y. Wan, H. Yang, D. Zhao. (2006). *Accounts of Chemical Research*, 39, 423-432.

13) P. Z.-Poor, A. Badiei, B. D. Fahlman, P. Arab, G. M. Ziarani. (2011). *Ind. Eng. Chem. Res.*, 50, 10036-10040.

14) B. G. Trewyn, I. I. Slowing, S. Giri, H.-T. Chen, V. S.-Y. Lin. (2007). *Acc. Chem. Res.*, 40, 846-853.

15) M. V.-Regi, F. Balas, M. Colilla, M. Manzano. (2008). *Progress in Solid State Chemistry*, 36, 163-191.

16) J. M. Rosenholm, M. Linden. (2008). *Journal of Controlled Release,* 128, 157-164.

17) S.-W. Song, K. Hidajat, S. Kawi. (2005). *Langmuir*, 21, 9568-9575.

18) M. N. V. Ravi Kumar. (2000). *JPPS*, 3, 234-258.

19) X. Huang, C. S. Brazel. (2001). *Journal of Controlled Release,* 73, 121-136.

20) A. K. Bajpai, S. K. Shukla, S. Bhanu, S. Kankane. (2008). *Progress in Polymer Science,* 33, 1088-1118.

21) T. M. Allen, P. R. Cullis. (2004). *Science,* 303, 1818-1822.

22) M. Vallet-Regi. (2006). *Chem. Eur. J.,* 12, 5934-5943.

23) D. C. Bibby, N. M. Davies, I. G. Tucker. (2000). *International Journal of Pharmaceutics,* 197, 1-11.

24) P. Yang, Z. Quan, C. Li, H. Lian, S. Huang, J. Lin. (2008). *Microporous and Mesoporous Materials,* 116, 524–531.

25) J. Lu, M. Liong, J. I. Zink, F. Tamanoi. (2007). *Small,* 3, 1341-1346.

26) T. Ukmar, O. Planinsek. (2010). *Acta. Pharm.,* 60, 373-385.

27) J. Liu, X. Jiang, C. Ashley, C. J. Brinker. (2009). *J. Am. Chem. Soc.,* 131, 7567-7569.

28) G. G. Liversidge, K. C. Cundy. (1995). *International Journal of Pharmaceutics,* 125, 91-97.

29) P. Zhao, H. Jiang, T. Jiang, Z. Zhi, C. Wu, C. Sun, J. Zhang, S. Wang. (2012). *European Journal of Pharmaceutical Sciences,* 45, 639-647.

30) B. Haley, E. Frenkel. (2008). *The Potential of Nanotechnology in Urologic Oncology,* 26, 57-64.

31) G. Chawla, P. Gupta, R. Thilagavathi, A. K. Chakraborti, A. K. Bansal. (2003). *European Journal of Pharmaceutical Sciences,* 20, 305-317.

32) A. Tan, A. K. Davey, C. A. Prestidge. (2011). *Pharmaceutical Research,* 28, 2273-2287.

33) A. Tan, S. Simovic, A. K. Davey, T. Rades, C. A. Prestidge. (2009). *Journal of Controlled Release,* 134, 62-70.

34) Y. Liu, C. Sun, Y. Hao, T. Jiang, L. Zheng, S. Wang. (2010). *Journal of Pharmaceutical Science,* 13, 589-606.

35) A. Tan, A. Martin, T.-H. Nguyen, B. J. Boyd, C. A. Prestidge. (2012). *Angewandte Chemie International Edition,* 51, 5475-5479.

36) D. Zhao, Q. Huo, J. Feng, B. F. Chmelka, G. D. Stucky. (1998). *J. Am. Chem. Soc.,* 120, 6024-6036.

37) M. Paul, N. Pal, A. Bhaumik. (2012). *Materials Science and Engineering C,* 32, 1461-1468.

38) F. F. Sevimli, *Surface Functionalization of SBA-15 Particles for Amoxicillin Delivery,* 2011, Thesis (MSc). Middle East Technical University.

39) I. Z.-Barba, S. S.-Salcedo, M. Colilla, M. J. Feito, C. R.-Santillan, M. T. Portoles, M. V.-Regi. (2011). *Acta Biomaterialia*, 7, 2977-2985.

40) D. H. Hwang, D. Lee, H. Lee, D. Choe, S. H. Lee, K. Lee. (2010). *Korean J. Chem. Eng.*, 27, 1087-1092.

41) K. Lee, D. Lee, H. Lee, C. K. Kim, Z. Wu, K. Lee. (2010). *Korean J. Chem. Eng.*, 27, 1333-1337.

42) R. F. Popovici, E. M. Seftel, G. D. Mihai, E. Popovici, V. A. Voicu. (2011). *Journal of Pharmaceutical Sciences*, 100, 704-714.

43) O. Glatter, O. Kratky. (1982). *In Small Angle X-ray Scattering*. London: Academic Press Inc.

44) A. Y. Khodakov, V. L. Zholobenko, M. I.-Clerc, D. Durand. (2005). *J. Phys. Chem. B*, 109, 22780-22790.

45) T. Kang, Y. Park, K. Choi, J. S. Lee, J. Yi. (2004). *J. Mater. Chem.*, 14, 1043-1049.

46) F. Sevimli, A. Yılmaz. (2012). *Microporous and Mesoporous Materials*, 158, 281-291.

47) P. I. Rayikovitch, A. V. Neimark. (2001). *J. Phys. Chem. B*, 105, 6817-6823.

48) A. Szegedi, M. Popova, I. Goshev, J. Mihaly. (2011). *Journal of Solid State Chemistry*, 184, 1201-1207.

49) Y.-Q. Xu, G.-W. Zhou, C.-C. Wu, T.-D. Li, H.-B. Song. (2011). *Solid State Science*, 13, 867-874.

50) T. Ukmar, U. Maver, O. Planinsek, V. Kaucic, M. Gaberscek, A. Godec. (2011). *Journal of Controlled Release*, 155, 409-417.

51) S. Inagaki, S. Guan, Y. Fukushima, T. Ohsuna, O. Terasaki. (1999). *J. Am. Chem. Soc.*, 121, 9611-9614.

52) H. Tuysuz, C. W. Lehmann, H. Bongard, B. Tesche, R. Schmidt, F. Schuth. (2008). *J. Am. Chem. Soc.*, 130, 11510-11517.

53) A. Yıldırım, E. Ozgur, M. Bayındır. (2013). *Journal of Materials Chemistry B*, 1, 1909-1920.

54) A. S Maria Chong, X. S. Zhao. (2003). *Journal of Physical Chemistry B*, 107, 12650-12657.

55) X. X. Yan, H. X. Deng, X. H. Huang, G. Q. Lu, S. Z. Qiao, D. Y. Zhao, C. Z. Yu. (2005). *Journal of Non-crystalline Solids*, 351, 3209-3217.

56) J. M Esparzaa, M. L. Ojedaa, A. Camperoa, A. Dom'ınguеza, I. Kornhausera, F. Rojasa, A. M. Vidalesb, R. H. Lopezb, G. Zgrablich. (2004). *Colloids and Surfaces A.*

57) S. P. Hudson, R. F. Padera, R. Langer, D. S. Kohane. (2008). *Biomaterials*, 29, 4045-4055.

58) J. M. Drazen. (2005). *The New England Journal of Medicine.*

59) A. Erdoğ, *Characterization of Liposomal Celecoxib Formulation as a Drug Delivery System in Colorectal Cancer Cell Lines*, 2012, Thesis (PhD). Middle East Technical University.

APPENDIX

UV ANALYSIS AND CALIBRATION CURVES OF CELECOXIB

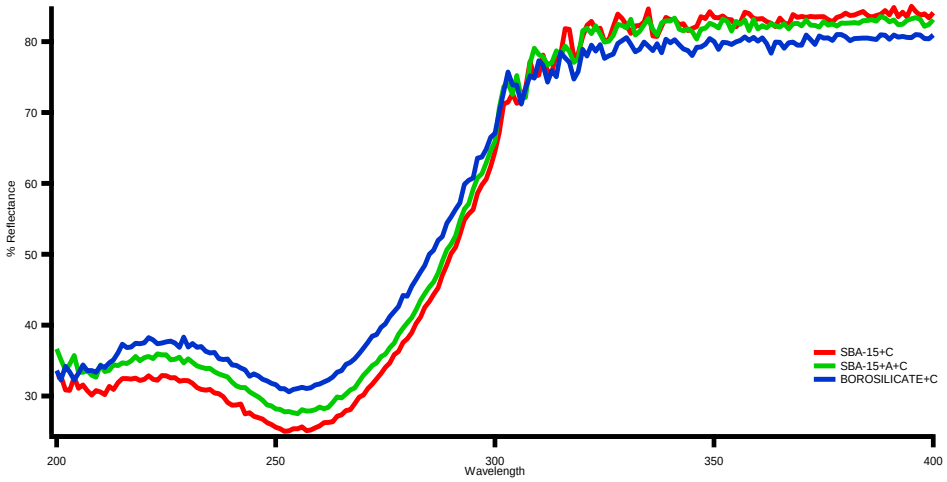

Figure-60: UV Analysis of Celecoxib Loaded Samples.

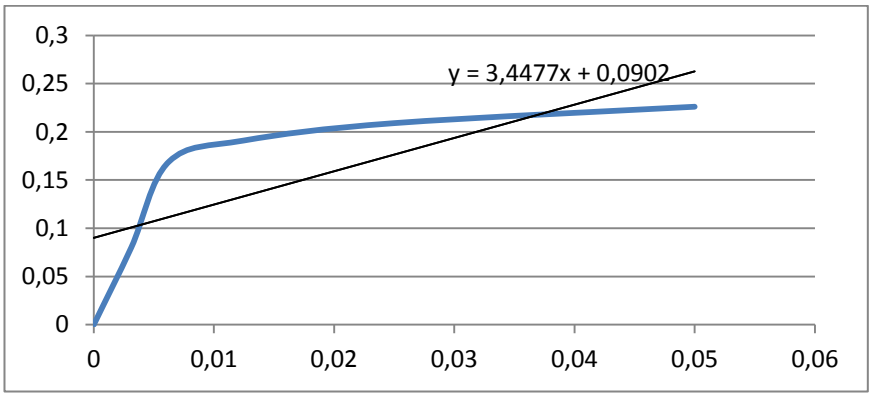

Figure-61: Calibration Curve of Loading Process of Celecoxib

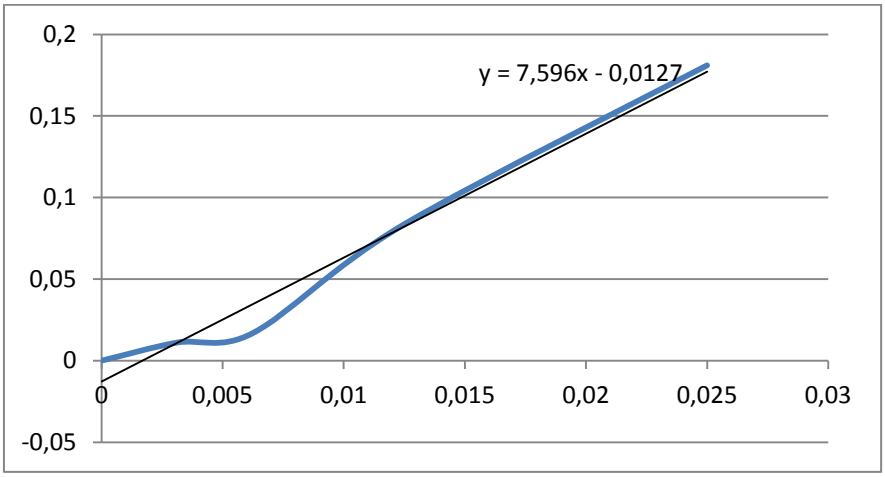

Figure-62: Calibration Curve of Release Process of Celecoxib